DETERMINATION OF THE THERMAL CONDUCTANCE OF THERMAL INTERFACE MATERIALS AS A FUNCTION OF PRESSURE LOADING

by

Benjamin N. Sponagle

Submitted in partial fulfillment of the requirements
for the degree of Master of Applied Science

at

Dalhousie University
Halifax, Nova Scotia
August 2012

DALHOUSIE UNIVERSITY
DEPARTMENT OF MECHANICAL ENGINEERING

The undersigned hereby certify that they have read and recommend to the Faculty of Graduate Studies for acceptance a thesis entitled "Determination of the Thermal Conductance of Thermal Interface Materials as a Function of Pressure Loading" by Benjamin N. Sponagle in partial fulfillment of the requirements for the degree of Master of Applied Science.

Dated: August 15, 2012

Supervisor: _____

Readers: _____

_____

DALHOUSIE UNIVERSITY

DATE: August 15, 2012

AUTHOR: Benjamin N. Sponagle

TITLE: Determination of the Thermal Conductance of Thermal Interface Materials as a Function of Pressure Loading.

DEPARTMENT OR SCHOOL: Department of Mechanical Engineering

DEGREE: MASc   CONVOCATION: October   YEAR: 2012

Permission is herewith granted to Dalhousie University to circulate and to have copied for non-commercial purposes, at its discretion, the above title upon the request of individuals or institutions. I understand that my thesis will be electronically available to the public.

The author reserves other publication rights, and neither the thesis nor extensive extracts from it may be printed or otherwise reproduced without the author's written permission.

The author attests that permission has been obtained for the use of any copyrighted material appearing in the thesis (other than the brief excerpts requiring only proper acknowledgement in scholarly writing), and that all such use is clearly acknowledged.

_____
Signature of Author

iii

TABLE OF CONTENTS

LIST OF TABLES

LIST OF FIGURES

ABSTRACT

This thesis presents an experimental apparatus and methodology for measuring the interface conductance of thermal interface materials (TIMs) as a function of clamping pressure. The experimental apparatus is a steady state characterization device based on the basic premise presented in ASTM D5470 – 06. The setup is designed to develop an approximately one dimensional heat transfer through a TIM sample which is held between two meter bars. The temperature is measured along the meter bars using resistance temperature detectors (RTDs) and the temperature drop across the interface is extrapolated from these measurements and then used to calculate the conductance of the interface.

This setup and methodology was used to characterize six commercial TIMs at pressures ranging from 0.17-2.76 MPa (25-400 psi). These TIMs included: Tgrease 880, Tflex 720, Tmate 2905c, Tpcm HP105, Cho-Therm 1671, and Cho-Therm T500. The measured conductance values for the various tests ranged from 0.19 to 5.7 W/cm^{2}K.

A three dimensional FEA model of the experimental setup was created in COMSOL Multiphysics 4.2a. This model was compared to the experimental data for a single data point and showed good correlation with the measured temperatures and conductance value.

LIST OF ABBREVIATIONS AND SYMBOLS

Abbreviations
TIM   Thermal Interface Materials
RTD   Resistance Temperature Detector
CMD   Coordinate Measuring Device
PCM   Phase Change Material
LMTA   Low Melting Temperature Alloy

Symbols
x x-coordinate (m)
y y-coordinate (m)
z z-coordinate (m)
A Interface area (cm^2)
d Position (m)
T Temperature (K)
Q Heat conduction (W)
k Thermal conductivity (W/m·K)
h Heat Transfer Coefficient

Greek Symbol
θ Contact conductance (cm^2 K/W)

Subscripts
C Cold side of the interface
H Hot side of the interface
$i{\rightarrow}j$ Difference calculated between location i and j
lateralheatloss   Heat losses through the sides of the insulating jacket
topheatloss   Heat losses through the top of the insulating jacket
heatsink   Heat sink properties

ACKNOWLEDGMENTS

Firstly, I would like to extend my thanks to my supervisor, Dr. Dominic Groulx, who has supported and encouraged my pursuit of research since I was an undergraduate intern in his lab. There is no question, that without his knowledge, patients and seemingly endless energy this thesis and research would never have been completed.

I would like to thank the members of my examining committee: Dr. Darrel Doman and Dr. George Jarjoura for generously providing me with their incites, suggestions as well as their time.

I would like to acknowledge everyone in the Mechanical Engineering Department who has helped me throughout this research. My special thanks go to Robert Warner, Peter Jones, Mark MacDonald, Albert Murphy and Jonathan MacDonald. I would also like to acknowledge my fellow researchers working at the Lab of Applied Multiphase Thermal Engineering.

The financial support for this project was received from Raytheon. My thanks go to John Jacobs and all of the Raytheon employees with whom I've corresponded for their support and technical advice.

I would like to take this opportunity to thank my family. The love, encouragement and advice that I have received from them throughout my life and during this research project can never be repaid.

Last but far from least I would like to thank my wife, Melissa. She has supported this work in too many ways to list and her compassion, understanding, and patience are my inspiration.

CHAPTER 1: INTRODUCTION

1.1 Background

Advances in design and manufacturing have allowed for the construction of increasingly small microchips. However, while their size has decreased the operating heat dissipation within microchips has increased. For instance, Pentium 2 CPUs have a die area of 25.4 mm^2 with a power dissipation of approximately 33W, while Pentium 4 CPUs have an effective die area of 16 mm^2 with a power dissipation of approximately 80 W. The increase in power coupled with the decreased heat transfer area results in an increased heat flux. Gwin and Webb (2003) approximate that from the Pentium 2 to the Pentium 4 the heat flux increased by a factor of 6.1. The heat dissipated in the microchip must be transferred from the chip to the heat sink so it can be expelled to the surroundings. Efficient removal of the dissipated heat is the key to managing the chips operating temperature. For heat to conduct to the heat sink it must be transferred across an interface between the heat sink, chip and heat spreader. This interface represents a resistance to heat transfer and can be quite significant (15-80% of the total resistance). Also, the interface resistance accounts for a higher percentage of the total thermal resistance as chip size decreases. (Gwin and Webb, 2003)

The resistance at an interface is the result of surface imperfections. Both of the surfaces which make up the interface will have a microscopic roughness and will not be perfectly flat. As a result, at a microscopic scale, the surfaces consist of a series of peaks and valleys. When the two surfaces are pressed together, the peaks and valleys interact producing interstitial air pockets (see Fig. 1.1).
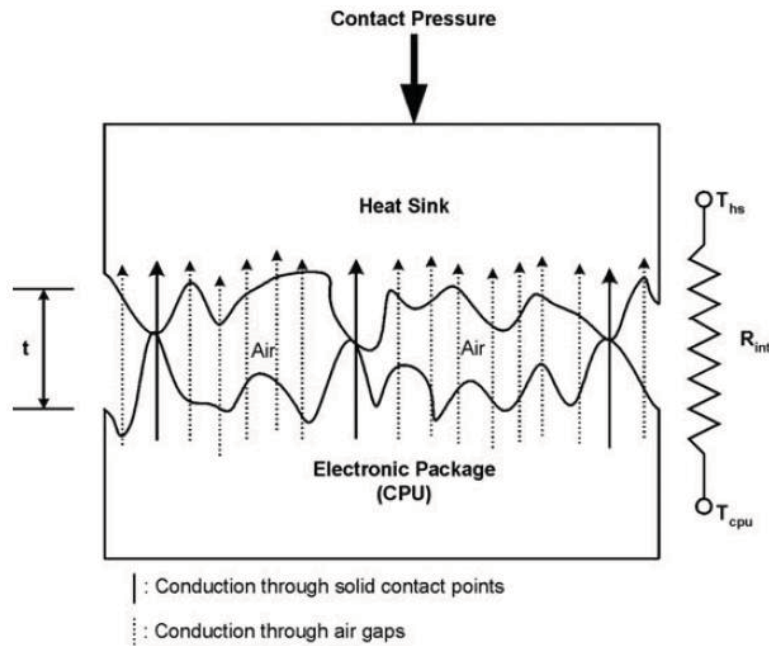
Figure 1.1 Illustration of Contact Interface (Gwin and Webb, 2003)

These air pockets have a high thermal resistance impeding heat conduction and effectively reducing the heat transfer area. One method for reducing the thermal resistance of an interface is to increase the surface contact area. Surface contact area can be increased by increasing the contact pressure: additional pressure will flatten the peaks of the surface roughness and deflect the surfaces to reduce the effect of non-flatness. Alternatively, the surfaces can be ground and buffed to reduce surface roughness and increase flatness. Finally, a thermal interface material (TIM) can be placed into the interface. The ideal TIM is a substance capable of filling the interstitial air pockets and having a high thermal conductivity to easily conduct heat. However, in reality some interstitial air will remain and a layer will be formed between the surfaces increasing the thickness of the interface (see Fig. 1.2).
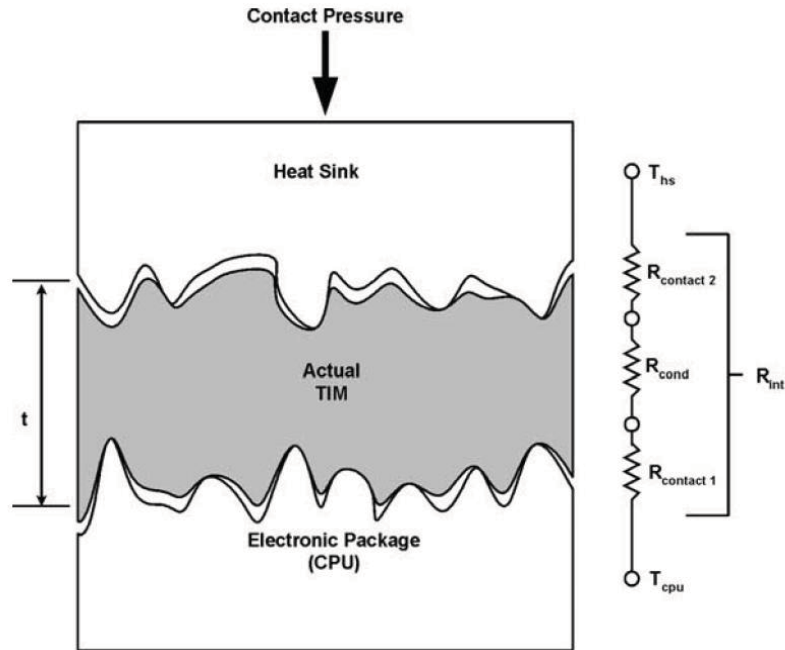
Figure 1.2 Illustration of TIM Layer Between an Interface (Gwin and Webb, 2003)

The thermal performance of a particular TIM is determined by three thermal resistance values. Two contact resistances where the TIM layer mates with the surfaces. These resistances are mainly controlled by the TIMs ability to conform to the surface asperities. Additionally, there is a thermal resistance associated with conducting heat across the TIM layer. This conduction resistance value is a function of the TIM layers thickness (often referred to as bond line thickness (BLT)) as well as the effective thermal conductivity of the TIM layer.

3

1.2 Thermal Interface Materials

There are many varieties of thermal interface materials available commercially and that have been investigated in literature. The majority of these consist of a deformable base with thermally conductive fillers suspended within. The base can be a liquid as with thermal greases or a deformable solid as with elastomer pads. Phase change materials are used as a compromise between these two technologies combining the benefits of both. Finally, there are more novel designs such as those based on carbon nano-tube technologies.

1.2.1 Thermal Greases/Pastes

Thermal greases consist of a mixture of two substances: a liquid polymer base and thermally conductive filler. Sarvar *et al.* (2006) cite silicone gel as being a commonly used base material. Fillers consist of small thermally conductive particles which are often made of ceramics or metals. Sarvar *et al.* (2006) lists several materials that have been used as thermally conductive fillers in thermal greases: alumina, aluminum nitride, zinc oxide, silicon dioxide, beryllium oxides, aluminum and silver. Xu *et al.* (2000) tested several different thermal greases and thermal pastes (see Table 1.1). The thermal pastes are similar to thermal greases in that they consist of a liquid base filled with thermally conductive particles, the only difference being the pastes use non grease base materials such as sodium silicate. Xu *et al.* (2000) conclude that the sodium silicate based TIMs have the highest contact conductance of those tested.

**Table 1.1 Contact conductance measurements for a variety of TIMs (W/cm^2 K) (Xu
et al., 2000)**

Thermal Interface Material	Contact Pressure (Mpa)				
	0.23	0.46	0.69	0.92	1.15
solder	20.8 ± 0.6	-	-	-	-
Sodium silicate /BN (18.0 vol. %)	13.2 ± 0.7	15.5 ± 0.9	16.9 ±0.3	14.3 ± 0.2	15.8± 0.2
Sodium silicate /BN (17.3 vol. %)	15.1 ± 0.5	15.5 ± 0.4	15.3 ± 0.4	16.4 ± 0.4	16.8 ±0.5
Sodium silicate /BN (16.0 vol. %)	18.6 ±0.7	18.2 ± 0.7	17.8 ± 0.7	17.7 ± 0.5	18.0 ± 0.7
Sodium silicate /BN (15.3 vol. %)	16.5 ± 0.3	16.3 ± 0.2	15.6 ± 0.2	16.5 ± 0.3	17.6 ± 0.4
Sodium silicate	14.0 ± 0.4	14.1 ± 0.5	15.0 ± 0.4	13.9 ± 0.6	14.0 ± 0.5
Water	11.7 ± 0.4	12.8 ± 0.4	-	-	-
Silicone/ZnO	11.2 ± 0.2	12.2 ± 0.6	13.7 ± 0.7	13.5 ± 1.6	12.3 ± 0.4
Silicone/BN	11.2 ± 0.7	10.9 ± 1.5	12.0 ± 1.5	13.4 ± 1.4	13.8 ± 0.6
Silicone	2.42 ± 0.04	3.08 ± 0.03	3.34 ± 0.05	4.05 ± 0.05	3.95 ± 0.10
Polymer/ZnO	5.22 ± 0.15	5.16 ± 0.09	5.45 ± 0.12	6.27 ± 0.17	5.91 ± 0.49
Perfluoropolyether	1.76 ± 0.15	2.81 ± 0.22	3.70 ± 0.20	4.65 ± 0.27	5.42 ± 0.45
Mineral oil	1.78 ± 0.05	1.70 ± 0.05	2.06 ± 0.22	1.92 ± 0.06	2.02 ± 0.14
Epoxy/graphite	0.988 ± 0.004	1.07 ± 0.01	1.31 ± 0.05	1.46 ± 0.08	1.48 ± 0.06
none	0.598 ± 0.004	0.68 ± 0.01	0.88 ± 0.04	0.99 ± 0.03	1.17 ± 0.05

Gwinn & Webb (2003) lists resistance values for several commercially available thermal
grease TIMs. These TIMs include aluminum and silver filled greases ranging from 0.018
– 0.387 K cm^2/W (55.5 – 2.58 W/cm^2 K). Xu *et al.* (2002) tested several different
compositions of a TIM with a polyethylene glycol base, a hexagonal boron nitride filler,
and additional lithium ions. The composition with the highest performance consisted of a
polyethylene glycol base with 1.5% by weight lithium salt (CF_3CO_2Li) and 18.0
volume% boron nitride particles mixed with water and N-dimethylforamide, the latter

two substances helping dissolve the lithium salt. This TIM composition was measured by the author to have a conductance of $(18.9 \pm 0.8) \times 10^4$ W/m^2 K $(18.9 \pm 0.8$ W/cm^2 K).

Gwinn & Webb (2003) lists the advantages of thermal greases/pastes:

- Thermal greases have excellent thermal performance without high pressures.
- They effectively fill the interstitial air pockets in the interface
- Joint pressure will cause the excess grease to flow from the interface producing a thin joint.
- No curing is required

The authors list the following disadvantages:

- Thermal greases are messy and may be hard to apply and remove.
- Joints require the use of hardware to maintain integrity.
- Excess grease that flows out of joint must be removed to avoid contamination or possible electrical shorts.
- Heat sink removal and reinstallation requires that the thermal grease is cleaned and then reapplied to the interface
- Thermal greases can be "pumped out" of the interface during thermal cycling as a result of the relative movement of the mating surfaces via thermal expansion and contraction.
- Thermal greases can dry out over time reducing their effectiveness.
- Thermal greases do not electrically insulate the two surfaces.

Sarvar *et al.* (2006) presents a similar list of advantages and disadvantages, also noting the low cost associated with thermal grease products.

Luo *et al.* (2001) studies the degradation of six different thermal paste formulations under different heating conditions (see Table 1.2 and 1.3). The author cycled the samples from 30 to 120°C at 10°C/ min for 6, 15 and 100 cycles as well as heating the sample to 100°C for 24 hours.

Table 1.2 Thermal conductance values with different thermal cycling conditions (W/cm² K) @ 0.46 MPa (Luo *et al.*, 2001)

	Before heating	After 6 cycles	After 15 cycles	After 100 cycles	After heating to 100°C for 24 hours
Silicone/ZnO	13.4 ± 0.7	13.4 ± 0.7	13.1 ± 0.6	13.1 ± 0.6	13.0 ± 0.5
PEG/BN(A)	18.9 ± 0.8	18.9 ± 0.8	18.0 ± 0.8	17.7 ± 0.7	12.3 ± 0.6
PEG/BN(B)	18.8 ± 0.8	18.7 ± 0.8	18.2 ± 0.7	18.0 ± 0.6	13.0 ± 0.7
PEG/BN(C)	14.9 ± 0.6	14.0 ± 0.6	14.0 ± 0.7	13.8 ± 0.6	11.2 ± 0.5
PEG/BN(D)	17.1 ± 0.5	16.0 ± 0.5	15.5 ± 0.5	15.0 ± 0.5	9.2 ± 0.4
Sodium Silicate BN	18.2 ± 0.7	18.1 ± 0.7	17.7 ± 0.7	17.2 ± 0.6	10.9 ± 0.8

Table 1.3 Composition of PEG/BN compounds tested by Luo *et al.* (2001)

	Lithium salt (CF3CO2Li) (wt%)	Boron nitride particles (wt%)
PEG/BN(A)	1.5	18.0
PEG/BN(B)	1.5	16.0
PEG/BN(C)	3.0	19.5
PEG/BN(D)	3.0	16.0

Luo *et al.* (2001) concludes that the silicone base thermal interface materials were the most thermally stable of the materials tested. The fractional reduction in conductance for the silicone based TIM was 2% for 100 cycles while for the other TIMs the conductance reduction was as large as 12%. For the isothermal heating case the silicone TIM's fractional decrease in conductance was again 2% while the other TIMs saw reductions as large as 46%. However, while the silicone materials were the most thermally stable of the tested materials the polyethylene glycol and sodium silicate based materials had greater or comparable conductance values even after heating.

1.2.2 Phase Change Materials

Phase change materials refer to those TIMs that are solid at room temperature but flow much like a thermal grease above a certain temperature threshold. Gwinn & Webb (2003) cites a phase change temperature between 50 – 90°C as typical. They also report that at a pressure of 0.068 MPa (9.9 psi), the highest performance PCM had a 40% higher

7

resistance than that of the best practical thermal grease. Liu & Chung (2006) conducted tests on a phase change material consisting of paraffin wax filled with boron nitride particles. They tested different percentages of filler from 0-8.6% by volume. The samples were also tested at different temperatures. They reported the performance of the TIM increased as the percentage of filler was increased from 0-6.2%, however, from 6.2-8.6% the performance decreased. The authors stated this was a reflection of the filler having two competing effects on the TIM. The more filler that is used the greater the conductivity of the mix but as the percentage of filler is increased so does the viscosity. Higher viscosity impairs the TIMs ability to conform to the mated surfaces. The highest conductivity measured above the melting point of the TIM by Liu & Chung (2006) was 18 W/cm^2 K.

Laird T-mate 2900, is a phase change material. The T-mate material consists of an unspecified phase change base which has a phase change softening temperature of 50-70°C. This base is filled with boron nitride particles and is reinforced with a metal foil. At 0.138 MPa (20.0 psi) the manufacturer claims a thermal resistance of 0.45 K cm^2/W (2.22 W/cm^2 K) (for the thinnest sheet having a thickness of 0.13mm). Gwinn & Webb (2003) lists a series of twelve commercially available materials and the manufacturer's values of thermal conductance (see Table 1.4). The resistances listed for phase change TIMs ranged from 0.142 to 0.645 K cm^2/W (7.04 to 1.55 W/cm^2 K). Gwinn & Webb (2003) and Sarvar *et al.* (2006) both reviewed the advantages and disadvantages of phase change TIMs. They both found that phase change materials are easier to handle than thermal greases and pastes as they consist of a solid pad at room temperature. Also, these materials generally do not suffer from pump out or dry out effects and have high thermal performance at moderate contact pressures. Disadvantages associated with phase change materials include the need for a constant clamping pressure much like greases. Also, Intel discourages the use of phase change materials because their characterization tests found them to have poor thermal properties (contrary to manufacturer values) and because they form a strong adhesive bond between the chip and heat sink and cause undesirable loads during drop and shock testing.

Table 1.4 List of Commercial Thermal Interface Materials and Properties (Gwinn & Webb, 2003)

Thermal Grease	Conductance (W/cm2K)	Pressure psi	Pressure MPa
Article silver	56	12	0.083
ShinEtsu G751	9.90	-	-
ShinEtsu G765	2.58	-	-
ShinEtsu G750	6.02	-	-
Berquist TIC-7500	4.42	50	0.345
Phase change materials			
Thermax HF-60110-BT	22	3-100	0.021-0.69
Power Strate 60 (AG)	7.04	10	0.069
Power Strate 50 (AF)	7.04	10	0.069
Chomerics T725	5.15	50	0.345
Orcus inc. FSF 52	5.15	4.5	0.031
Chomerics T454	3.88	50	0.345
Thermagon T-pcm 905c	3.16	10	0.069
Berquist HighFlow	3.10	-	-
Berquist 200U	3.88	10	0.069
Berquist HiFlow 225-U	1.94	10	0.069
Berquist HiFlow 225-UT	1.72	10	0.069
Chomerics T443	1.55	50	0.345

An alternative type of phase change material is low melting temperature alloys (LMTAs). These TIMs are essentially solder alloys that are chosen to have a melting point lower than the operating temperature of the application. Sarvar *et al.* (2006) lists the following as commonly used metals: bismuth, indium, gallium and tin. Carlberg *et al.* (2009) developed and tested a TIM consisting of a porous polymeric structure, manufactured from a thermoplastic elastomer via electrospinning, impregnated with an LMTA. The LMTA used is a eutectic alloy of In, Bi and Sn which has a melting temperature of 60°C. They tested the TIM at pressures of 0.2-0.8 MPa (29-116 psi) and measured resistances as low as 8.5 K mm^2/W (11.8 W/cm^{2}K).

1.2.3 Thermally Conductive Elastomers

Thermally conductive elastomers consist of an elastomer filled with thermally conductive particles. These elastomers are sometimes referred to as gels and are generally silicone based. Elastomer pads are often reinforced with either dielectric films or fibreglass (Sarvar *et al.*, 2006 and deSorgo, 1996). These materials do not flow freely but when pressure is applied they deform to fill the interstitial gaps. Pressure must be maintained with hardware. DeSorgo (1996) found that a pressure of 2.07 to 3.45 MPa (300 to 500 psi) was required to fill the interstitial gaps. Gwinn & Webb (2003) found that the pressure required for thermally conductive elastomers was unacceptably high for CPU cooling applications.

Two of the materials listed in the Raytheon work order fall into the classification of thermally conductive elastomers. Chomeric's CHO-THERM® T500 consists of a silicone elastomer filled with boron nitride particles and reinforced with fiber glass. The published thermal interface resistance for this material is 1.23 K cm^2/W (0.81 W/ cm^{2}K) with a 0.25 mm thick sample at an unspecified pressure. CHO-THERM® 1671 is a similar product manufactured with the same materials and having a published interface resistance of 1.48 K cm^2/W with a 0.38 mm thick sample at an unspecified pressure. Elastomer pad TIMs are generally electrically insulative unlike thermal greases and phase change materials and are easy to handle during installation and removal due to the fact that they are solid pads. Additionally, these materials do not suffer from pump out or dry out problems and cannot leak out of the interface. However, thermally conductive elastomers have poor thermal performance at low pressures (Sarvar *et al.*, 2006).

1.2.4 Carbon Based Thermal Interface Material

The state of the art in thermal interface materials revolves around the use of carbon nanotubes. Carbon nanotubes (CNTs) can refer to single walled or multi walled hollow carbon tubes. Single walled structures consist of a single sheet of carbon atoms (graphene) rolled up to form a tube with a diameter in the order of 1 nm. Multi walled structures consist of several sheets rolled into concentric tubes with a diameter in the order of 10 nm (Sarvar *et al.*, 2006). Individual multi walled CNTs can have thermal conductivities from 600-3000 W/m·K with films of vertically aligned CNTs having effective thermal conductivities of 15-200 W/m·K. These high conductivities have attracted researchers to CNTs for TIM applications (Gwinn & Webb, 2003). Liu et al. (2004) randomly dispersed a mixture of both single walled and multi walled CNTs in a silicone elastomer. They found, as the amount of CNTs was increased the thermal conductivity was increased and at 3.8% by weight CNTs the thermal conductivity of the elastomer was enhanced by 65%. An elastomer filled with the same weight percent of carbon black was tested and saw a smaller increase. Park & Taya (2006) tested a TIM consisting of CNTs dispersed randomly in a silicone grease (chloroform was used as a solvent). The author reports that the mixture had a thermal resistance of 0.0265–0.0399 K cm^2/W (37.7–25.1 W/cm^{2}K). Xu & Fisher (2006) grew an array of carbon nanotubes on a silicon substrate using microwave plasma-enhanced chemical vapour deposition. This array of vertically aligned CNTs was tested as a TIM using a steady state test method; the author additionally tested the array in combination with an Indium sheet and a PCM (Honeywell PCM45F). The CNT array alone was measured to have a minimum thermal resistance of 19.8 K mm^2/W (5.05 W/cm^{2}K) at 0.445 MPa (64.5 psi). The combination of CNT array and indium sheet was only slightly better than the indium sheet alone which was measured to be between 27.2 and 18.5 K mm^2/W (3.68 and 5.41 W/cm^{2}K). The combination of CNT array and PCM had the lowest resistance, measured to be 5.2 mm^2 K/W (19 W/cm^{2}K) at 0.35 MPa (51 psi). Zhang *et al.* (2008) grew a similar array of nanotubes on a silicon substrate via microwave plasma-enhanced

chemical vapour deposition. The thermal resistance of the CNT TIM was measured to be 7 mm^2 K/W (14 W/cm^{2}K) at 0.15 MPa (22 psi).

1.3 Steady State Characterization

Methods for measuring the thermal resistance or conductance of a TIM filled interface can be separated into two broad categories: steady state and transient. A steady state characterization system is described by ASTM D5470 – 06 "Standard Test Method for Thermal Transmission Properties of Thermally Conductive Electrical Insulation Materials". The standard describes a system where the TIM sample is placed between two thermally conductive (conductivity>50W/m·K) cylinders referred to as meter bars. The temperatures of each of the meter bars should be taken at, at least, two different locations along their length. A heat source is applied to one side of the assembly and a heat sink to the opposite (see Fig. 1.3).

```
┌─────────────┐
│    Heat     │
│   Source    │
├─────────────┤
│     T1      │
│  Hot Meter  │
│    Bar      │
│     T2      │
├─────────────┤
│  Specimen   │
├─────────────┤
│     T3      │
│    Cold     │
│  Meter Bar  │
│     T4      │
├─────────────┤
│    Heat     │
│    Sink     │
└─────────────┘
```
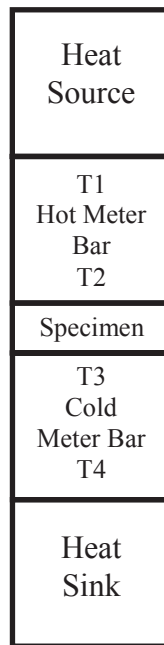
Figure 1.3 Steady State Test Schematic (ASTM D5470 – 06)

After the system is brought to steady state the temperature measurements can then be used to determine both the heat flow through the meter bars and the resistance of the

sample. The following equations are given to calculate the heat flow through the meter bars.

$$Q_{12} = \frac{k_{12}A}{d}[T_1 - T_2] \tag{1.1}$$

$$Q_{34} = \frac{k_{34}A}{d}[T_3 - T_4] \tag{1.2}$$

$$Q = \frac{Q_{12} + Q_{34}}{2} \tag{1.3}$$

Where the temperatures (T_1, T_2, T_3, T_4) are those given in Fig. 1.3, Q_{12} is the heat flow through the hot meter bar, Q_{34} is the heat flow through the cold meter bar, and k_{12} and k_{34} are the conductivity of the bottom and top meter bars respectively.

The temperatures at the surface of the sample (T_H and T_C) can be derived from the temperature gradient in each of the meter bars and then can be used to calculate the thermal resistance of the sample layer given the following equations.

$$T_H = T_2 - \frac{d_B}{d_A}[T_1 - T_2] \tag{1.4}$$

$$T_C = T_3 - \frac{d_D}{d_C}[T_3 - T_4] \tag{1.5}$$

$$\theta = \frac{A}{Q}[T_H - T_C] \tag{1.6}$$

13

Where, d_A, d_B, d_C, and d_D are the distance between T_1 and T_2, the distance from T_2 to the sample surface, the distance between T_3 and T_4, and the distance from T_3 to the sample surface respectively.

ASTM D5470 – 06 describes an alternative method for measuring heat flow if an electrical heat source is used; the heat flow can be determined from the power supplied to the heater ($Q=IV$). However, if this method is used then insulation and guard heaters are required to avoid heat losses.

The standard states that the TIM sample should be tested under pressures ranging from 0.069 to 3.4 MPa (10 to 490 psi) depending on the material being tested. The test should also be completed at an average sample temperature of 50 °C.

Finally, the standard describes a method for measuring the contact resistance separately from the bulk resistance. This can be done by plotting the resistance of the TIM as a function of thickness. The thickness of the sample is either controlled via shims or varying pressure. The trend line "y" intercept estimates the resistance of a zero thickness sample or the contact resistance.

Lasance *et al.* (2006) review the advantages and disadvantages of the steady state method. They note that the steady state method has the advantage of being widely used by TIM suppliers as well as being mathematically simple. However, the steady state method described by ASTM D5470 uses meter bars with smooth surfaces which results in underestimations of the contact resistance. Lasance *et al.* (2006) conclude that steady state methods are best suited for standardized tests such as those conducted by manufacturers but that the transient method is better suited to application specific testing.

Smith *et al.* (2009) describes the limits of the steady state test. They state that the temperature rise across the TIM should be larger than the precision of the temperature sensors (in an example they use 50 times as large). If the TIM represents a large percentage of the assemblies combined resistance then maintaining a temperature difference across the TIM that is large in comparison to the sensor precision is feasible.

14

However, if the TIM represents a small percentage of the total assembly resistance then a large temperature difference between the heat source and sink will be required to maintain an acceptable temperature gradient across the TIM. Therefore, the precision of this test will tend to decrease as the performance of the TIM increases. Smith *et al.* (2009) also discusses the problems associated with the variable sample thickness method described in the ASTM standard. This method uses little data processing; however it requires measurements at variable sample thicknesses, referred to as bond line thickness (BLT) by the author. Smith *et al.* (2009) finds that it is not realistic to precisely control the BLT over a large range (5-100 μm) without artificial means to stop the bond line (*i.e.* the use of shims or other spacers) which can affect the measured values. This results in the accuracy of this method decreasing with range, and making it especially difficult to make accurate readings with samples of low viscosity. The difficulties associated with the variable BLT method do not affect the tests ability to make measurements of the total resistance of the sample (contact resistance and sample resistance combined) and Smith *et al.* (2009) find that a single resistance measurement at a design BLT thickness is the most relevant result of this test.

Authors have used measurement devices similar to the ASTM standard but with modifications. Lee *et al.* (1997) built a device very similar to that described in the ASTM standard but with four temperature sensors instead of two in each of the meter bars. The authors use a least square fit to calculate the heat flow through the assembly. Park & Taya (2006) use a custom manufactured thermister device to make the temperature measurements. The temperature sensor consists of layers of TiW and Au deposited onto an aluminum substrate (see Fig. 1.4). A thermister is similar to a resistance temperature detector (RTD). Both sensors consist of an element whose resistance changes with temperature. The distinction being that RTDs are generally constructed of pure metals (often platinum of nickel) and have a positive temperature coefficient; meaning their resistance increases with increasing temperature. Thermisters elements are made of more complex materials and can have a positive or negative temperature coefficient.
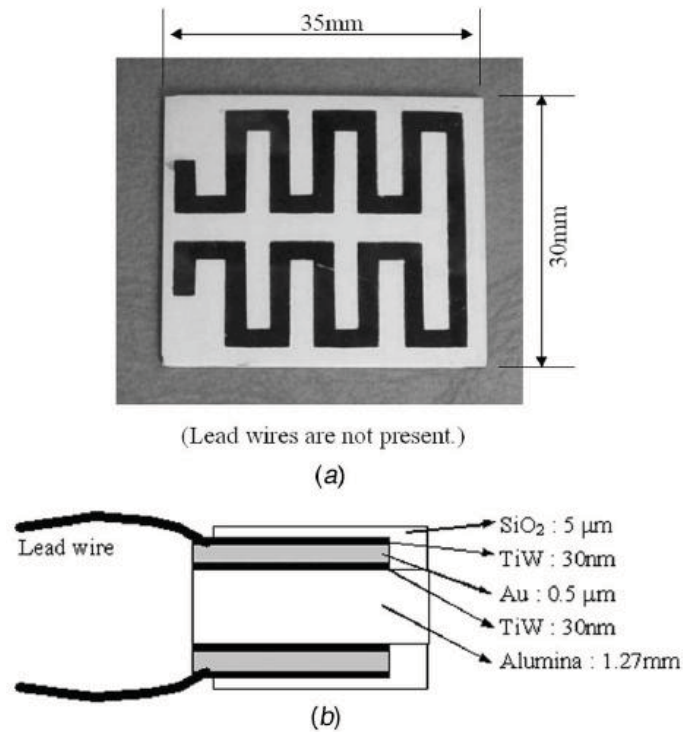
Figure 1.4 Thermister Sensor Schematic (Park &Taya, 2006)

The authors claim that this sensor is thinner than a thermocouple and effectively averages the temperature of the surface rather than measuring a point temperature like a thermocouple. The device depicted in Fig. 1.4 is used as the meter bars in the experiment with the TIM sample sandwiched between two such devices.

The contact resistance of a TIM layer is affected by the surface properties of the materials it is in contact with. If the TIM is tested using polished copper calorimeters the contact resistance may be underestimated (Lasance *et al.,* 2006). Zhang *et al.* (2008) modifies the standard method so that the TIM resistance can be measured in contact with different materials and surfaces. The authors make three separate measurements. First the TIM is sandwiched between plates of whatever material is of interest, in this case the TIM is placed between a silicon and aluminum plate (the TIM in question is a carbon nano-tubule construction and is actually grown on the silicon plate). This assembly is then

16

placed between two copper meter bars. The test can then be completed as per the standard procedure. This produces a total resistance for the assembly including the unknown contact resistance between the silicon and the meter bar and the aluminum and the meter bar. The authors then measure the resistance of only the silicon and only the aluminum and this allows them to determine the two unknown contact resistances and subtract them from the first measurement.

1.4 Transient Characterization

Lasance *et al.* (2006) reviewed the advantages and disadvantages of the transient method. They found it was easier to build an accurate test apparatus using the transient method. They also state that the transient method is faster and inherently more accurate because the whole temperature-time curve can be used for fitting. However, the disadvantage being that the parameter estimation from the temperature-time curve is much more difficult mathematically than in the case of the steady state test. Parker *et al.* (1961) presents a commonly used transient test method called the laser flash method. Clark & Taylor (1975) and Baba (2001) subsequently improve and modify the original method to account for heat losses. The laser flash method consists of placing the desired sample in front of a laser. The laser pulse is used to produce an impulse heating of one side of the assembly. The temperature at the opposite side of the assembly is then recorded. Parker *et al.* (1961) uses an equation for the temperature of an insulated solid given by Carslaw and Jaeger (1959) and the impulse initial condition to derive the following relationship.

$$\alpha = (1.38L^2/\pi^2 t_{1/2})$$

(1.7)

Where α is the thermal diffusivity of the sample and $t_{1/2}$ is the time it takes for the temperature-time curve to rise half way to its maximum. Clark & Taylor (1975) and Baba (2001) introduce a number of modifications to improve the method describes by Parker *et al.* (1961). These modifications include using an analytical model which accounts for radiation losses, using a fiber optic device to ensure that the laser pulse is uniform, and the use of curve fitting techniques instead of indicator values such as $t_{1/2}$.

Researchers at the Composite Materials Research Laboratory, State University of New York at Buffalo have published a number of papers using the laser flash method to characterize different TIMs. Luo *et al.* (2001), Xu *et al.* (2000), Liu & Chung (2006) and Xu *et al.* (2002) use a method very similar to that used by Parker *et al.* (1961). The TIM is places between two copper plates (much thinner than the meter bars used in the steady state test at ~1 mm thick). The laser flash is directed at one end of the assembly and the temperature of the other side is monitored with a thermocouple. The method for estimating the material properties from this time curve is not explicitly described, beyond mentioning that the finite element program ABAQUS was used. Liu & Chung, (2006) uses a similar laser flash technique to Luo *et al.* (2001), Xu *et al.* (2000), and Xu *et al.* (2002) and reports that they used $t_{1/2}$ as an input to the ABAQUS program, possibly indicating that a similar approach to Parker *et al.* (1961) was used. Liu & Chung, (2006) expands on the method used in Xu *et al.* (2000) and Xu *et al.* (2002) by adding a preheating furnace. This allowed the researchers to preheat the TIM sample before each test and get a variety of data points at different sample temperatures. Lasance *et al.* (2006) describes two systems which use a similar transient scheme to the laser flash method but use an electric heater and water impingement heating in place of the laser.

Each of the above devices produces a temperature-time curve. There are different schemes for estimating the material properties from this curve. The approach used by Parker *et al.* (1961) is based on an analytical model and uses $t_{1/2}$ as the measured value. Smith *et al.* (2009) uses two different methods to extract the thermal resistance of the TIM from the temperature-time curve. One method they used was to fit the experimental curve to one produced using a numerical model. The author was able to fit the experimental curve to a model with 3.3% relative error over the entire curve. They did, however, find that the curve was not particularly sensitive to changes in the TIM conductance when compared to other parameters in the analytical model. Smith *et al.* (2009) also discusses the use of structure functions to extract the TIM properties. The idea behind the structure function approach is that the test assembly (assuming one dimensional heat transmission) is analogous to an array of resistors in series. Using an

approach presented in detail in Szekel (1998) the response of series of resistors can be modeled using a convolution integral. So given a response curve and the input into the series of resistors a differential approach can be used to extract the structure of the array of resistors. This technique has the advantage of being able to measure the contact resistances of the TIM separately from the resistance associated with the BLT. Smith *et al.* (2009) found that the values produced by the two transient tests agreed with one another but were different from those found with a steady state tester and those supplied by the manufacturer.

1.5 Scope of the Thesis

The work presented in this thesis focuses on the development of an experimental setup and systematic methodology for the determination of the interface conductance of thermal interface materials as a function of clamping pressure. While the scope of this work only concerns the characterization of these materials as a function of clamping pressure considerations were made during design stage, for future work in characterizing TIMs as a function of temperature. The setup and methodology developed were used to characterize the performance of six commercially available TIMs: Tgrease 880, Tflex 720, Tmate 2905c, Tpcm HP105, Cho-Therm 1671, and Cho-Therm T500.

Ultimately, the goal of the work presented in this thesis was to establish an understanding of the many variables associated with the characterization of TIMs and how the different aspects of the experimental design impact the uncertainty and repeatability of the measurements.

Chapter 2 will present the experimental setup and equipment. Each of the TIMs to be tested will be introduced and discussed in this chapter. The manufacturer published conductance values for each of the TIMs is also presented here. Finally, a detailed step by step procedure used during the testing of TIM samples will be presented.

Chapter 3 will detail the calculation method used to obtain the interface conductance from the collected data. The estimation of the experimental uncertainty will also be presented along with a detailed sample calculation.

The results of the conductance measurements made using the six TIMs are summarized in Chapter 4. How the conductance values changed with clamping pressure is also discussed. Practical observations about each of the TIMs physical characteristics are presented in this chapter.

A three dimensional FEA model of the experimental setup is discussed in Chapter 5. By fitting three heat transfer coefficients, the simulation produces very similar temperature and conductance results to the experimental setup, for a single set of data (no TIM in the interface at 0.5 MPa (73 psi).

Chapter 6 contains the concluding remarks and a discussion of future work which could be done to expand on the work presented in this thesis.

CHAPTER 2: EXPERIMENTAL SETUP AND METHODOLOGY

The experimental apparatus and test methodology are described in this chapter. This includes a detailed description of the apparatus' construction and design as well as a step by step walk through of a typical test procedure. Also, included in this chapter is a review of the various TIMs that were tested. Their composition, physical characteristics and manufacturer published performance are discussed.

2.1 Experimental Setup and Instrumentation

The experimental setup uses the steady state method of characterization. It is based on the basic premise presented in ASTM D5470 – 06. The setup can be divided into two main sections: the test assembly and the press. The test assembly is the core of the experiment; all heat transfer is located within this section. The test assembly includes three main components: the meter bars which form the interface, the heating block, and the heat sink. During a measurement of interface conductance a TIM sample is placed between the meter bars. The heating block and heat sink are located on either side of the meter bars and are used to setup a steady state heat transfer through the meter bars and the TIM sample. The outside of the test assembly is insulated to approximate a one dimensional heat transfer. Figure 2.1 shows a simplified schematic of the test assembly's basic components.
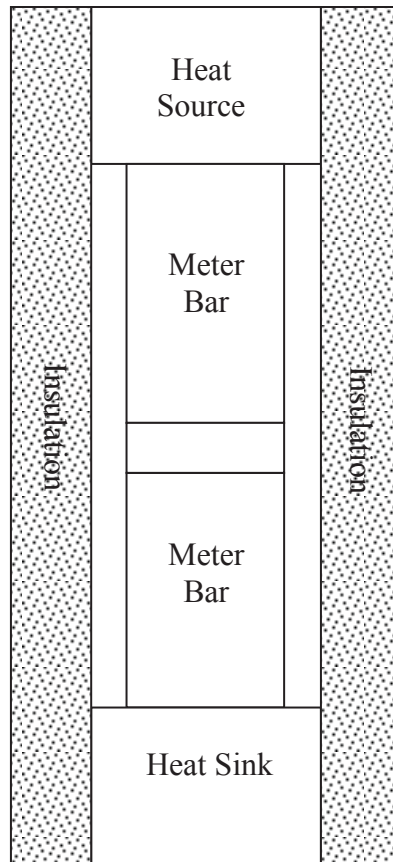
Figure 2.1 Simplified schematic of the test assembly

Each meter bar is a 51 mm by 25 mm by 25 mm (2" by 1" by 1") block of Al 6061 T6 aluminum alloy. Therefore, there is a one inch square test area to hold the sample TIM during testing. The temperature of the meter bars are measured using platinum Resistance Temperature Detector (RTD) sensors at three different locations along their length. They are placed in 15.9 mm (5/8") deep holes drilled into the side of the meter bars. The holes are filled with Laird T-Grease thermal paste before the sensors are inserted. The meter bars with the RTDs inserted are shown in Fig. 2.2.
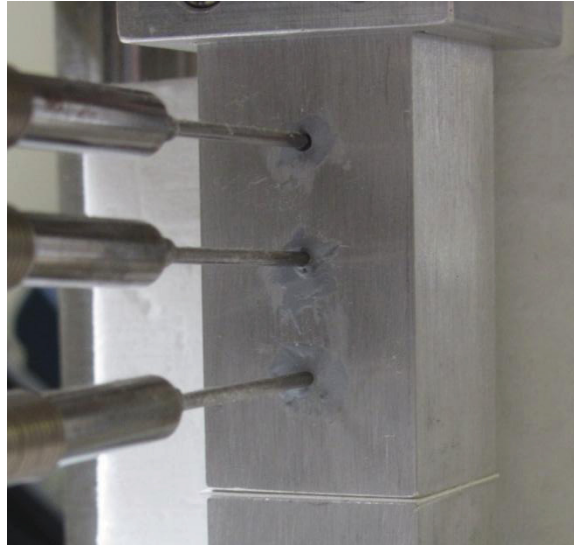
Figure 2.2 Photograph of the meter bars with the RTDs inserted

The locations of each of the holes along the meter bar were measure using a coordinate measuring device (CMD). How the holes were measured is illustrated in Fig. 2.3 and the measured values are shown in Table 2.1.
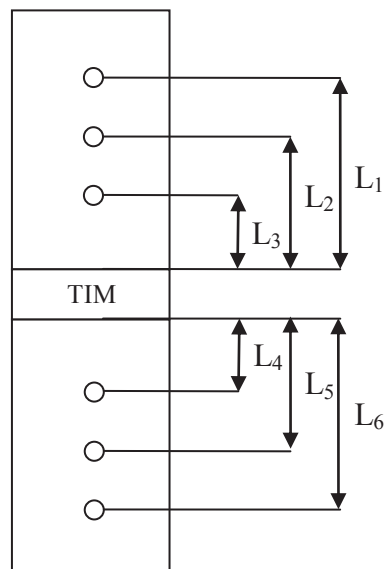
Figure 2.3   Illustration of CMD measurement methodology

Table 2.1 CMD Measurements having an absolute uncertainty of ± 0.01 mm

	CMD Measurement (mm)
L_1	38.03
L_2	25.35
L_3	12.62
L_4	12.58
L_5	25.29
L_6	38.00

The test surface of each of the blocks was machined to a #6 machine finish using a rotory grinder. The surface roughness (Ra) of the two blocks was measured to be 0.88±0.1 μm and 0.65±0.1 μm.

The heater block consists of two 50 W cartridge heaters which were inserted into an Al 6061 T6 aluminum block. There is a shallow recess machined on the bottom of the heater block into which the meter bar can be placed. This recess facilitates the alignment of the assembly.   A guard heater is employed above the heater block. This guard heater is identical to the experimental heater block and is separated from the test assembly by a layer of MACOR ceramic insulation. The voltage supplied to the test heater is controlled using a variable transformer (variac), while the guard heater is controlled using a solid state voltage controller. The cooler is a custom aluminum heat sink through which air is blown using a computer fan during testing. The heat sink was machined from an Al 6061 T6 aluminum block. As with the heater block the heat sink has an alignment recess machined into its top surface. The heater block and the heat sink are shown in Figs. 2.4 and 2.5 respectively.
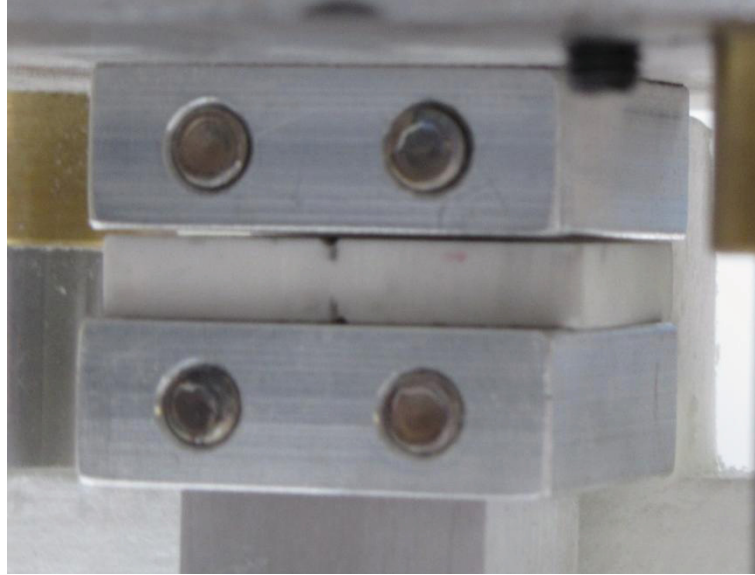
Figure 2.4 Photograph of the heater block and guard heater

Figure 2.5 Photograph of the heat sink

The outside of the assembly is insulated using ceramic fiber insulation. This ceramic fiber insulation was chosen because it is formed into ridged panels that could be assembled around the test assembly without physically touching the meter bars. This allowed for a controlled air gap between the insulation and the meter bars. Also, it was rated for use up to 900°C so there was no concern of it failing during testing. Figure 2.6 shows the entire test assembly with the partially assembled insulation blocks. Small cracks between the blocks are covered with tape during testing to ensure there is no air flow.

Figure 2.6 Photograph of partially assembled insulation blocks

In order to test samples at different clamping pressures a custom press was designed and built to fit the test assembly. The press consists of two sliding plates which move freely on four guide posts. Pressure is applied via a manual screw. The pressure is measured using a load cell located below the bottom sliding plate. Figure 2.7 shows a simplified schematic of the test press, this schematic is not to scale and is meant only to illustrate its major components and function.   Figure 2.8 shows a photograph of the experimental setup without insulation.
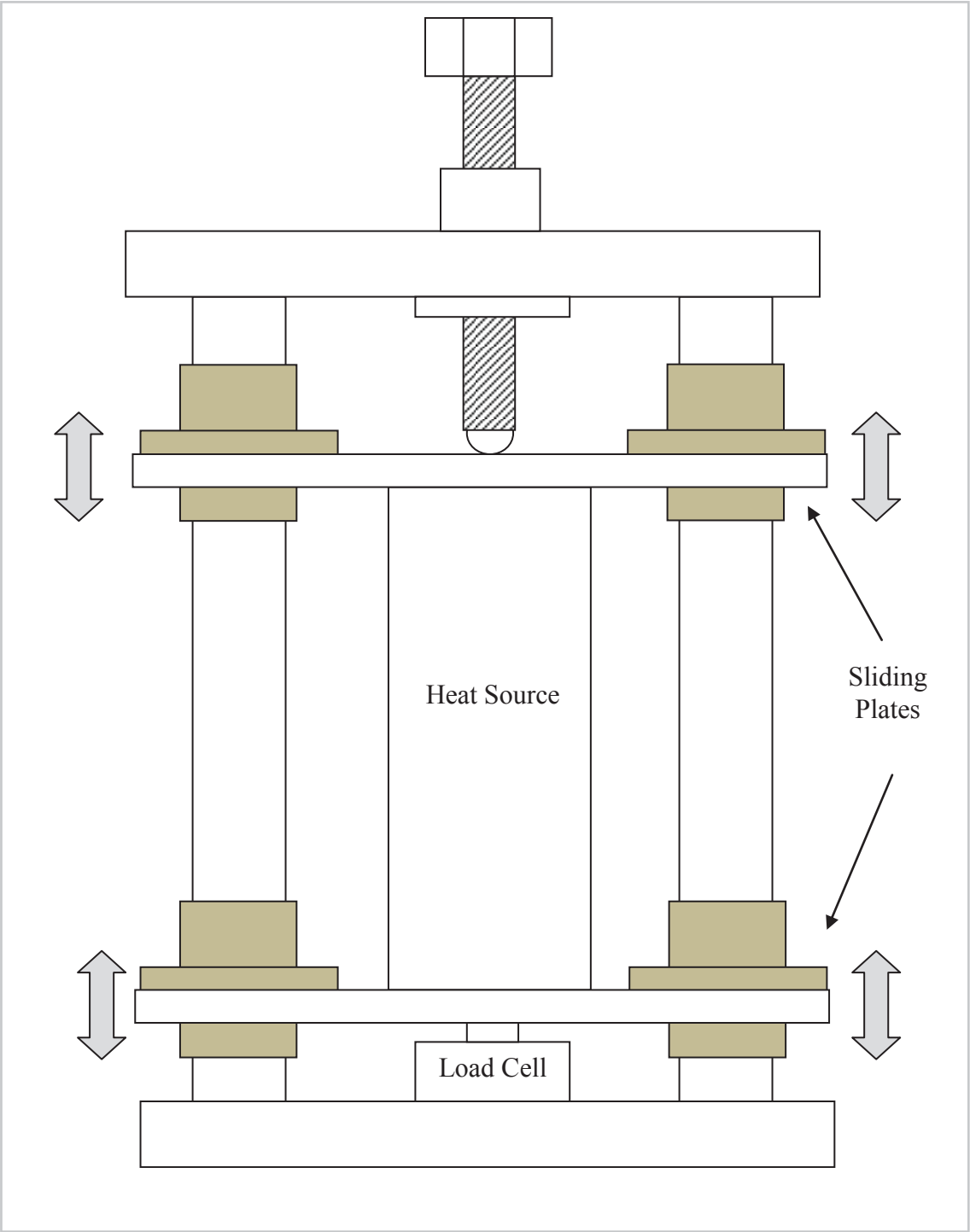
Figure 2.7 Simplified schematic of the test press
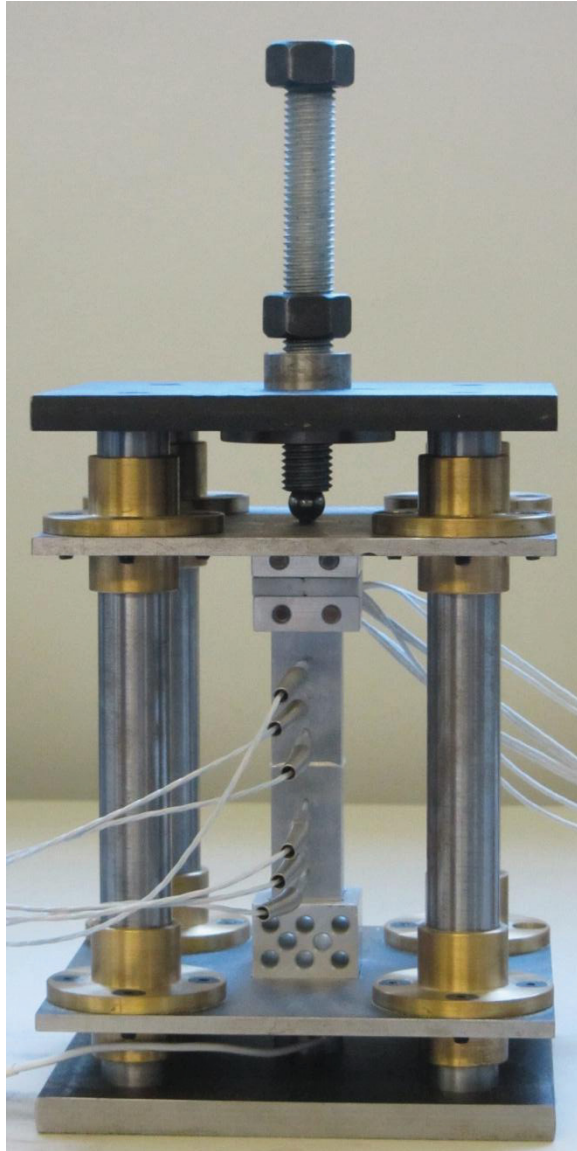
Figure 2.8 Photograph of the experimental setup without insulation

Table 2.2 gives additional details on the various components of the experimental setup. In addition to the hardware above a National Instruments Compaq DAQ was used to record the output from the various sensors. Four cards were used in the modular Compaq DAQ system. The universal NI 9219 module was used to record the output of the load cell. Two NI 9217 RTD modules were used to record the output of the six RTDs. Finally, one NI 9213 Thermocouple module was use to record the outputs of several thermocouples.

Table 2.2 Specifications of experimental setup components

Platinum RTDs	
Manufacturer	Omega
Part #	PR-11-2-100-1/16-2-E
Length	3"
Diameter	1/16"
Accuracy	Class A
Load Cell	
Manufacturer	Omega
Part #	LC304-500
Output	2mV/V
Accuracy	±0.5% Full Scale Output linearity, hysteresis, repeatability
Cartridge Heaters	
Manufacturer	Omega
Part #	CIR-1016/120V
Wattage	50 W
Fiber Board Insulation	
Manufacturer	Thermal Ceramics
Product Name	Superwool 607
Thermal Conductivity	0.06 W/mK
Thickness	1"
Ceramic Insulation	
Manufacturer	Corning
Product Name	MACOR
Thermal Conductivity	1.46 W/mK
Thickness	1/4"
Meter Bars	
Dimensions	2"×1"×1"
Material	Al 6061 T6
Thermal Conductivity	167 W/mK*

* American society for metals, ASM International.
Handbook Committee (1990)

2.2 Temperature Sensor Calibration

Platinum RTD sensors have a temperature varying accuracy. Class "A" RTDs have a tolerance of ±0.15 and ±0.35°C at 0 and 100°C respectively. In order to ensure that the probes were as accurate as possible, the probes used in these experiments were recalibrated using a FLUKE 7102 Micro calibration bath (see Table 2.3 for relevant specifications).

Table 2.3. Specification of the calibration bath used

Calibration Bath	
Manufacturer	FLUKE
Absolute Tolerance	±0.25 ˚C
Uniformity	±0.02 ˚C
Stability	0.015 ˚C @ -5˚C
	0.03 ˚C @ 121˚C
Fluid	5010 silicone oil

The important temperature measurements that must be made during the characterization of TIMs are all differential measurements. As a result, the interchangeability of the sensors is more important than the absolute uncertainty. As a result, a relative calibration was carried out. One of the RTDs in question was chosen as the standard and correction curves were produced for each of the other sensors to ensure they were all interchangeable. All of the sensors were placed in the bath and temperature readings were made using the same DAQ system and specific channels that would be used in the experiment. Thirteen measurements were made in total increasing from 50 to 115°C in 5 degree intervals. The sensors can then be corrected to be interchangeable within the stability tolerance of the bath. This was done by calculating the required adjustment for each sensor at each data point and then fitting a curve which related the required correction factor to the output of each sensor. This will not account for non-linearity or hysteresis errors associated with the sensors. It will however, account for any consistent bias between the sensors. It will be assumed that calibration bias over the small temperature differences measured is the major contributor to the error. Theoretically the uncertainty in the temperature differences between the RTDs would then be twice the uniformity of the bath or ±0.04°C. Actually comparing the sensors after the correction curve the difference between any of the sensors does not exceed 0.05°C. The value of ±0.05°C will be used in the calculations as the uncertainty associated with the calculated temperature differences.

2.3 Thermal Interface Materials

Six thermal interface materials were chosen for testing. They include commercial products from both Laird Technologies and Chomerics. There are representatives of the three most common categories: thermal greases, phase change materials, and elastomer pads.

2.3.1 Tgrease 880

Tgrease 880 is a thermal grease manufactured by Laird Technologies. The exact make up is not published but it most likely consists of silicone grease filled with thermally conductive filler. It is a liquid at room temperature and has a viscosity of <1500 Pa·s. Its interface conductance is given as a function of clamping pressure by Laird (see Table 2.4). Its performance is quite high. A notable feature of the published conductance values is that after approximately 0.069 to 0.10 MPa (10 to 15 psi) it increases very linearly with clamping pressure. Figure 2.9 is a photograph of the Tgrease as it was received from Laird Technologies.

Table 2.4 Laird Technologies published thermal conductance values for Tgrease 880

Applied Pressure MPa (psi)	Interface Conductance (W/cm^{2}K)
0.069 (10)	11
0.14 (20)	15
0.34 (50)	17

Figure 2.9 Tgrease 880 as received from the manufacturer

31

2.3.2 TFlex 720

TFlex 720 is a Laird Technologies product and is described by the manufacturer as gap filler. It is most similar to elastomer pad products but has the consistency of soft clay. It consists of a silicone base and ceramic filler. It is very soft and pliable. The sample tested had an initial thickness of 0.5 mm. The conductance values received from a Laird Technologies representative are shown in Table 2.5. Figure 2.10 is a photograph of the TFlex 720 as it was received from Laird Technologies.

Table 2.5 Laird Technologies thermal conductance values for TFlex 720 (I. Bryson, personal communication, June 11, 2012)

Applied Pressure MPa (psi)	Interface Conductance (W/cm^{2}K)
0.069 (10)	0.62
0.21 (30)	0.68
0.34 (50)	0.74
0.52 (75)	0.78
0.69 (100)	0.82
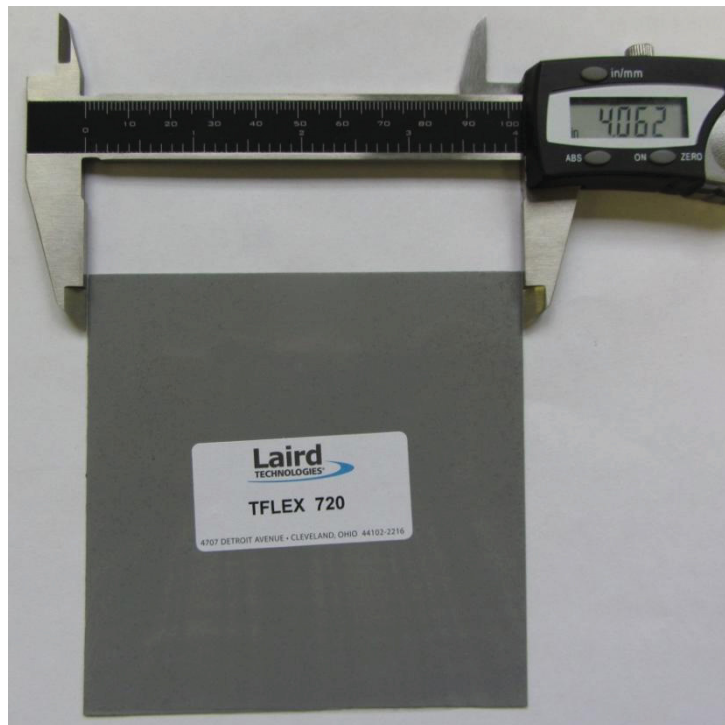
Figure 2.10 TFlex 720 as it was received from the manufacturer

2.3.3 Tmate 2905c

Tmate 2905c is a reinforced phase change material. It consists of a metal foil with a phase change material on one side of the foil. The base phase change material is not known but it is filled with ceramic boron nitride particles. This is a unique construction, among the materials tested, as only one side of the interface is in contact with the actual TIM; the other is in contact with the metal foil. The phase change material was a bright yellow colour and was very soft and pliable. The "phase change softening temperature" published by Laird Technologies is 50 to 70°C. It is not clear from the wording of the technical specification sheet if the phase change material will have made a full phase transition at these temperatures or if it will have only become more pliable. Only one conductance value is quoted in the technical specification sheet: at 0.14 MPa (20 psi) the thermal conductance is quoted as 2.2 W/cm^2K. The sample tested was 0.13 mm thick before testing. Figure 2.11 is a photograph of the Tmate 2905c as it was received from Laird Technologies.
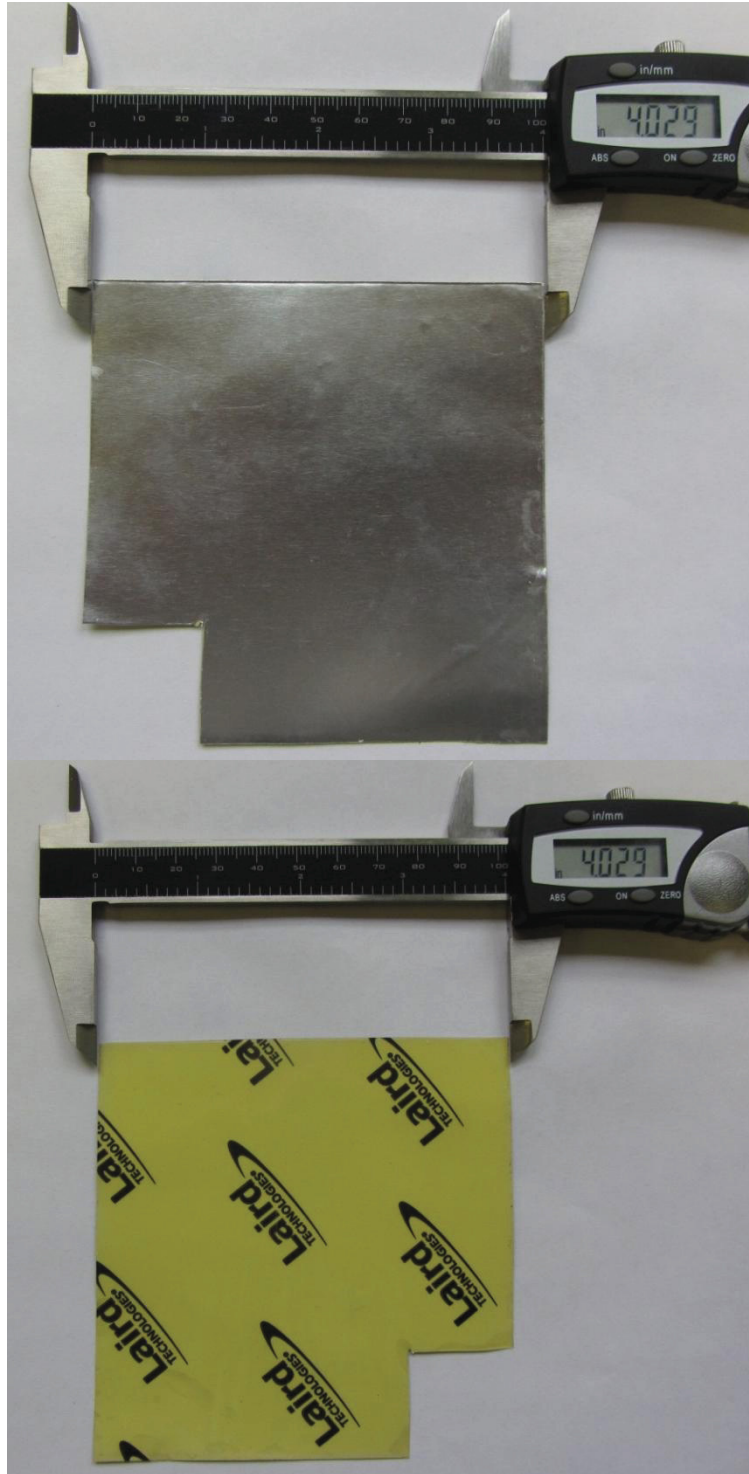
Figure 2.11 Tmate 2905c as it was received from the manufacturer with one sample having been removed for testing

2.3.4 Tpcm HP105

Tpcm HP105 is another phase change TIM manufactured by Laird Technologies. It is not reinforced with foil as with Tmate 2905c it is simply a thin layer of PCM. The base PCM is not known but it is filled with boron nitride particles. This material was difficult to handle as it was quite fragile and less pliable than the other tested TIMs. It was very easy to break a sample into pieces while attempting to place it between the meter bars. The phase change softening temperature is published as 50 to 70°C. The conductance values from the Laird Technologies spec sheet are summarized in Table 2.6. Figure 2.12 is a photograph of Tpcm HP105 as it was received from Laird Technologies.

Table 2.6 Laird Technologies published thermal conductance values for Tpcm HP105

Applied **Pressure MPa (psi)**	Interface Conductance (W/cm^{2}K)
0.069 (10)	6.7
0.34 (50)	9.1
0.69 (100)	10
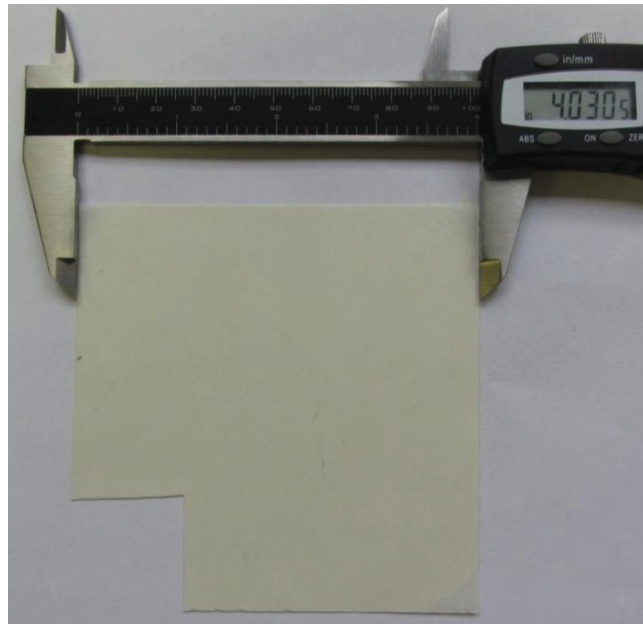
Figure 2.12 Tpcm HP105 as it was received from the manufacturer with one sample having been removed for testing

35

2.3.5 Cho-Therm 1671 & T500

Cho-Therm 1671 and T500 are both elastomer pad TIMs manufactured by Chomerics. Both of these products consist of a silicone elastomer base filled with boron nitride particles and reinforced with fiberglass. These materials are much tougher than any of the other TIMs. They do not appear pliable to the touch. Table 2.7 summarizes the specifications of these very similar TIM products. Note that the specification sheet for these materials does not quote a clamping pressure under which the conductance values were tested. However, the specification sheet does quote the ideal clamping pressure for these products as between 2.07 and 3.45 MPa (300 and 500 psi). Figures 2.13 and 2.14 are photographs of Cho-Therm 1671 and T500 respectively.

Table 2.7 Chomerics published thermal conductance values for Cho-Therm 1671 & T500

	Cho-Therm 1671	Cho-Therm T500
Interface Conductance (W/cm^{2}K)	0.676	0.813
Thickness (mm)	0.38	0.25
Colour	White	Green
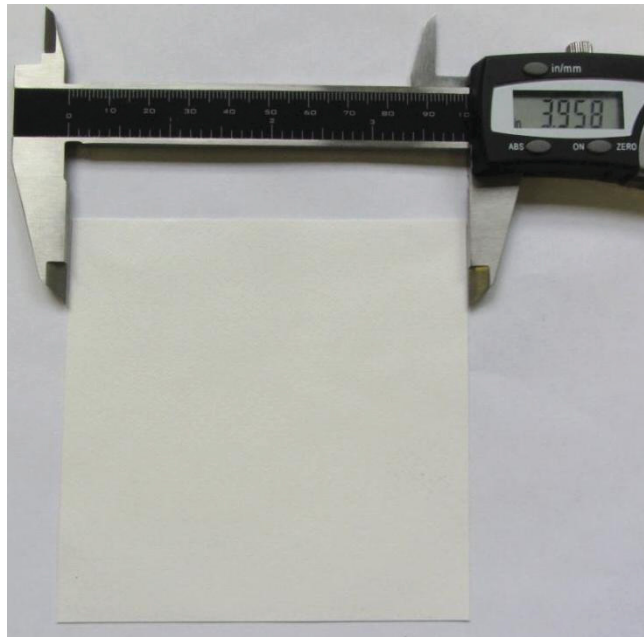
Figure 2.13 Cho-Therm 1671 as it was received from the manufacturer
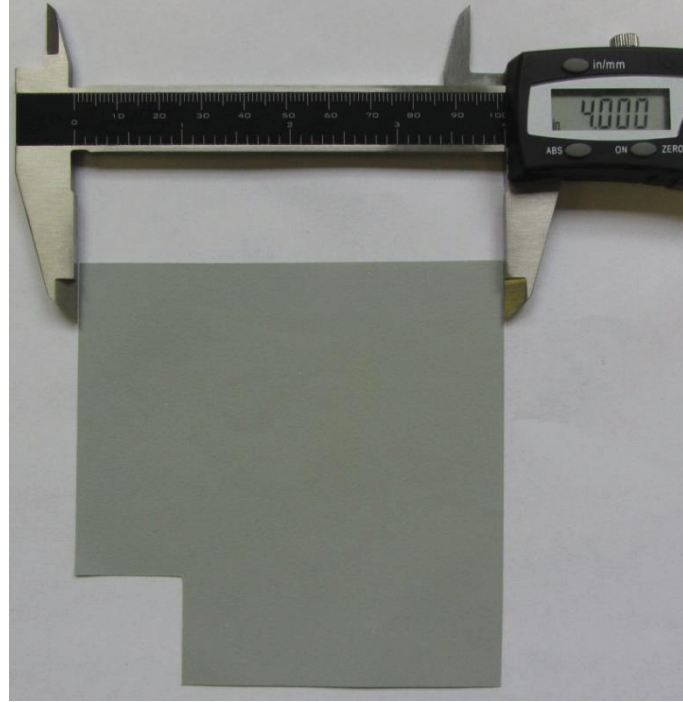
Figure 2.14 Cho-Therm T500 as it was received from the manufacturer with one sample having been removed for testing

2.4 Experimental Procedure

A sample of TIM is applied to the interface between the two meter bars at the beginning of each test. With the exception of the Tgrease 880 sample, all of the other TIMs are pads. This means that in order to apply them a 25mm by 25mm (1" by 1") sample is cut, from the ~102 mm by 102 mm (4" by 4") pads received from the manufacturers, and then placed into the interface between the meter bars. The Chomerics products are robust and not tacky or adhesive; they were received with minimal packaging. A sample of the material was cut from the sheets received from the manufacturer and easily placed in the interface. However, the three Laird pad type TIMs came packaged with a plastic or paper film to protect and reinforce them. This film had to be peeled off before the sample was placed in the interface (see Fig. 2.15).

37

Figure 2.15 Photograph of the packaging associated with the Laird Technologies pad type TIMs

The grease sample was applied by first spreading it onto one of the meter bars. The TIM was applied generously to ensure complete coverage (approximately 1 mm thick). When the second meter bar was placed on top and then placed into the test press a small pressure was applied (~0.1 MPa or 15psi).   This squeezed excess TIM out of the interface. This initial excess was wiped up before testing. During the test as the pressure was increased additional TIM was squeezed out of the interface, however, this proved to be a very small amount.

Once the test assembly is aligned within the press the heating block and cooling fan are turned on. The nominal voltage applied to the test heaters is 40 VAC, at this voltage the heater produced approximately 10 W of power. This voltage was chosen as it maintained the operating temperature in the range of 50-70°C.   This temperature range is high enough to melt the phase change material TIMs being tested, and also is in the same range as an operating CPU, which is a common application for TIMs.   The system is

allowed to reach steady state with no pressure being applied via the press. There is a small pressure associated with friction as the test assembly thermally expands and pushes the sliding plates. This pressure is kept at less than 0.14 MPa (20 psi). The system is assumed to be at steady state when consecutive temperature readings taken at two minute intervals show a temperature change of less than 0.05ºC. The time required to reach steady state was variable between tests but was generally in the range of 1 to 2 hours. When steady state is reached, pressure is applied to the system. The system is then allowed to achieve a new equilibrium state and a data point is recorded. Labview 2010 is used in consort with the National Instruments Compact DAQ system to manage the data collection. Data is collected for ten minutes at 4 Hz. Pressure measurements are made in parallel with the temperature measurements utilizing the same DAQ system. Additionally, the voltage and current being supplied to the heater are measured during each data point using multimeters wired into the system. The temperature difference between the guard heater and the experimental heater is measured using two type T thermocouples which are inserted on either side of the MACOR insulation. The temperature difference across this insulation layer is kept below ± 0.2°C during each data point measurement. This procedure is then repeated increasing the applied pressure each time. The time that it takes for the system to reach equilibrium after a pressure change depends on the specific TIM and pressure, but generally would take between 15-40 minutes.

When the clamping pressure is increased it was observed that the pressure would then decrease from the initial peak pressure. In some cases the pressure would relax by as much as 0.14 MPa (20 psi). This is likely a result of two processes. In the case of highly deformable TIMs, material will flow out of the interface when the clamping pressure is increased. This flow out of material accounts for some of the pressure relaxation. This theory is reinforced by the fact that the pressure relaxation is more pronounced for Tflex 720, Tmate 2905c, and Tpcm HP105. These materials are soft enough to flow out of the interface at higher clamping pressures. The pressure relaxation when testing the pad materials and Tgrease 880 was smaller. The pads do not flow and the majority of the

Tgrease 880 flows out of the interface as soon as a small pressure is initially applied. Secondly, because the conductance of the interface increases with pressure the average operating temperature of the whole assembly will decrease with each increase in pressure. This cooling of the test assembly results in a thermal contraction reducing the applied pressure. During testing the pressure is set to the desired pressure for the data point and then it is allowed to relax. Then the pressure is reset to the data point pressure. This is repeated several times until the pressure remains stable at the desired value. This could be a source of error in the experiment as it is easy to overshoot the desired pressure while resetting the pressure screw several times.

Once equilibrium is achieved and the data point is recorded the result is ten minutes of temperature and pressure data. This data is exported from Labview as text files. These text files are then read by a program written in Matlab script which calculates the interface conductance for each of the clamping pressures. Before the calculations are completed each of the data points is visually examined to confirm the system was at steady state and that there were no aberrations in the data. In a small number of cases the system fluctuated from steady state at the beginning or end of the ten minute period. When this was the case the unsteady data was simply removed before calculating the conductance values. The Matlab program used for calculation of the conductance values is included in appendix A.

CHAPTER 3: CALCULATION OF INTERFACE CONDUCTANCE

The calculation of the interface conductance is based on the ASTM D5470 – 06 method that was previously presented in chapter one. It makes the assumption that the system can be approximated as being one dimensional. In other words the heat flux through any cross section of the meter bars is perfectly uniform. Heat losses through the sides of the test assembly and non-uniform heating or cooling of either end of the assembly will contribute to experimental bias. Equation (3.1) is the core relation used to calculate the interface conductance.

$$\theta = Q A^{-1} (T_H - T_C)^{-1}$$

(3.1)

where T_H and T_C are the temperatures at the hot and cold side of the interface. However, measuring the temperature at the two sides of the interface directly is difficult. The interface thickness will be a fraction of a millimeter so placing sensors in the interface is not feasible. Instead of directly measuring T_H and T_C they are extrapolated from the temperature gradient within the meter bar. Holes are drilled into the meter bars and RTDs are used to measure the temperature at each of these points. Holes are not placed close to the interface as this could affect the interface surface and distort the results. Knowing temperature measurements and the locations of those readings, the gradient in the meter bars and therefore the temperature drop across the interface can be calculated. The temperature drop can then be used with Eq. (3.1) to solve for conductance (see Fig. 3.1).

$$\Delta T_{H \to C} = \Delta T_{3 \to 4} - d_{3 \to H} \left(\frac{dT}{dz} \right)_{hot} - d_{C \to 4} \left(\frac{dT}{dz} \right)_{cold}$$

(3.2)

$$\left(\frac{dT}{dz} \right)_{hot} = \frac{\Delta T_{1 \to 3}}{d_{1 \to 3}}$$

(3.3)

41

$$\left(\frac{dT}{dz}\right)_{cold} = \frac{\Delta T_{4\to5}}{d_{4\to5}} \qquad\qquad (3.4)$$
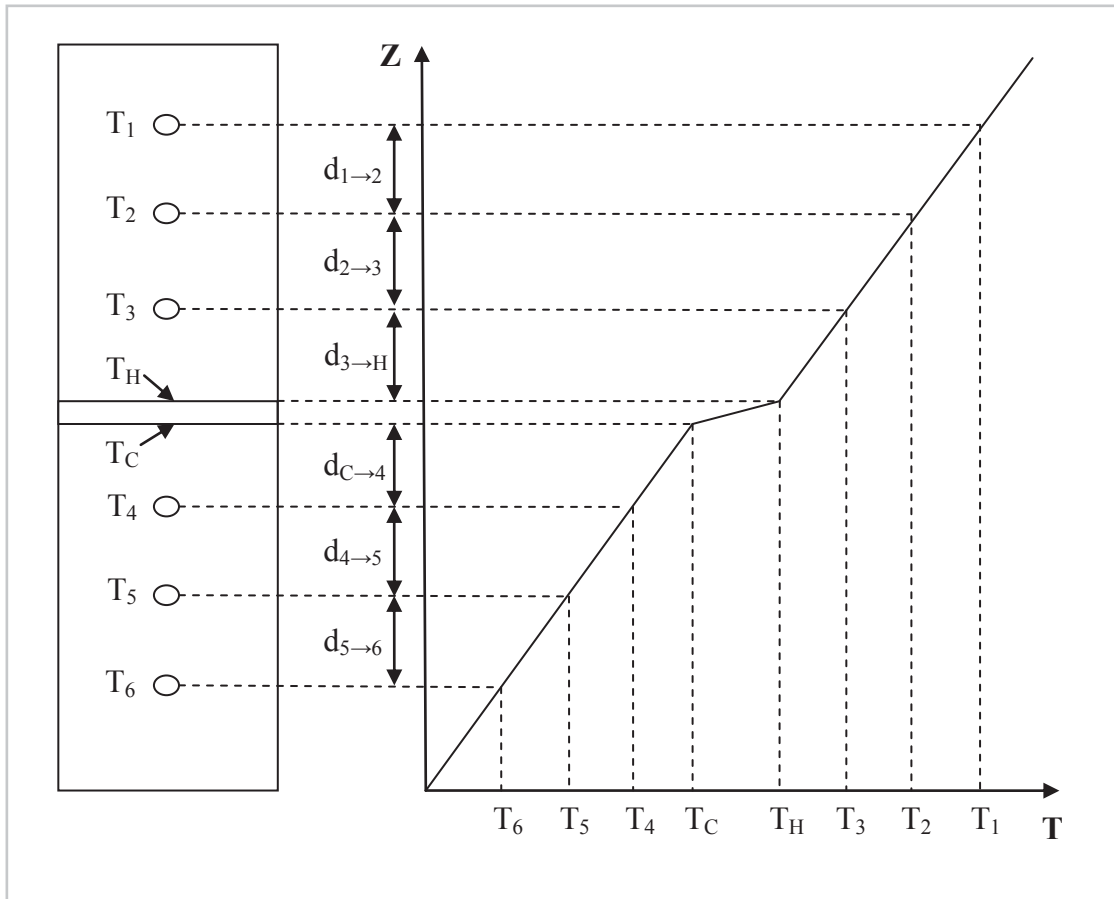
Figure 3.1 Illustration of the theory behind the one dimensional heat transfer method of calculating interface conductance

Figure 3.1 illustrates the method shown in Eqs. (3.2) to (3.4) for extrapolating the interface surface temperatures from the temperature measurements along the meter bars. Given the thermal conductivity of the meter bars k the heat flux through the test assembly can be calculated using Eq. (3.5). Equation 3.6 shows the resulting relationship for conductance, note that the area of the interface A is present in Eqs. (3.1) and (3.5) and can be cancelled out of the final relation.

$$Q = kA \left[\frac{\left(\frac{dT}{dz}\right)_{hot} + \left(\frac{dT}{dz}\right)_{cold}}{2} \right] \qquad (3.5)$$

$$\theta = \left[\frac{k}{2} \left(\left(\frac{dT}{dz}\right)_{hot} + \left(\frac{dT}{dz}\right)_{cold} \right) \right] \left[\Delta T_{3 \to 4} - d_{3 \to H} \left(\frac{dT}{dz}\right)_{hot} - d_{C \to 4} \left(\frac{dT}{dz}\right)_{cold} \right]^{-1} \qquad (3.6)$$

Figures 3.2 and 3.3 show a set of data that was taken while running a test at 0.50 MPa (73psi) with no TIM sample in the interface. Both show 10 minutes of data that was taken at 4 Hz. This set of data will be used as a case study for demonstrating and expanding upon the above calculations.

The first step is to convert the data into differential temperature measurements. This will generate sets of differential temperature data: $\Delta T_{1 \to 3}, \Delta T_{3 \to 4}, \Delta T_{4 \to 6}$.
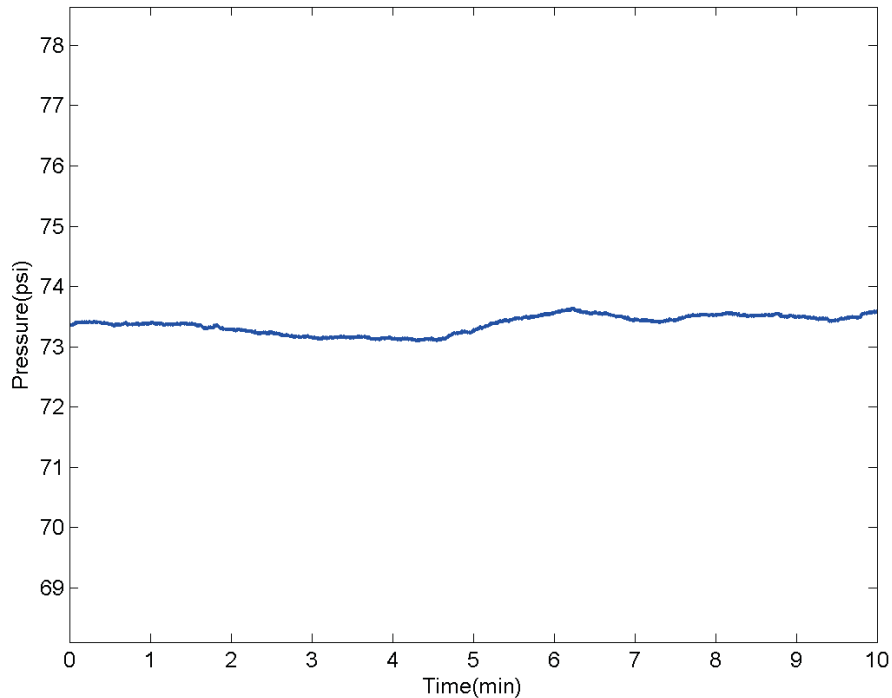
Figure 3.2 Pressure data collected during testing with no TIM sample at 0.50 MPa (73psi). The uncertainty on the pressure measurement is ± 0.02 MPa (± 2.5 psi).

43
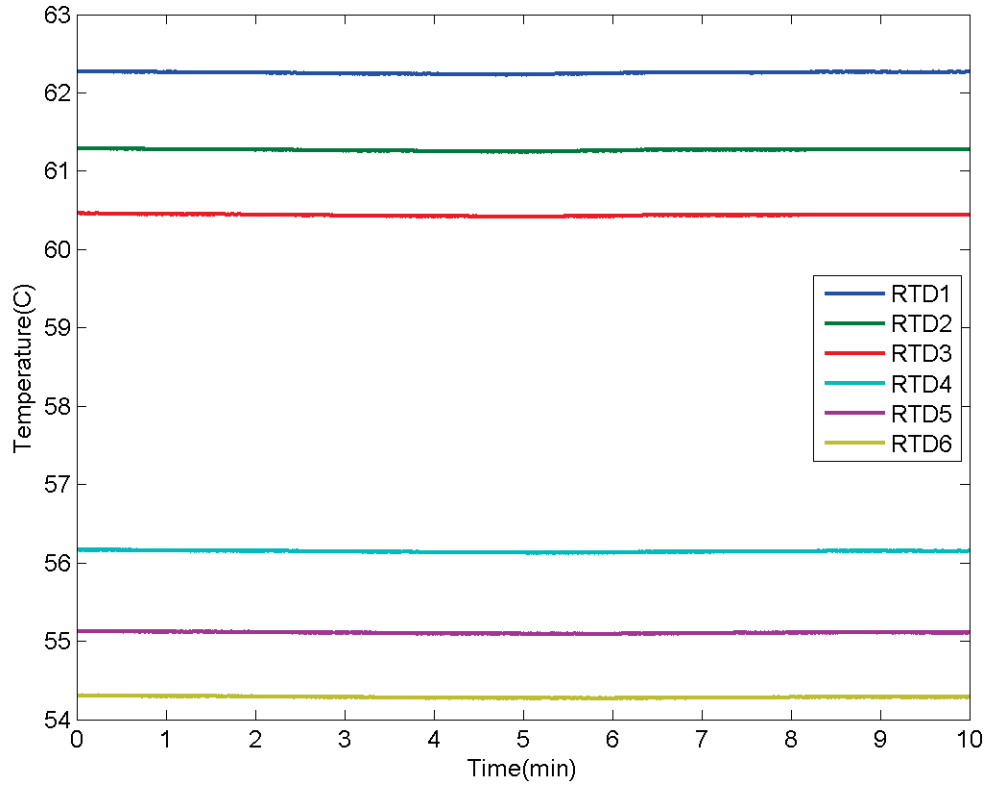
Figure 3.3 Temperature data collected during testing with no TIM sample at 0.50 MPa (73psi)

A mean value of each of the differential temperature measurements and a mean value of the pressure is calculated. Using Eq. (3.7) the random uncertainty ($P_{\Delta T}$) in the differential temperature data can be calculated.

$$P_{\Delta T} = \frac{1.96 \times \sigma_{\Delta T}}{\sqrt{n_{\Delta T}}} \; [K] \tag{3.7}$$

Where $\sigma_{\Delta T}$ is the standard deviation of the dataset and $n_{\Delta T}$ is the number of data points in the dataset. The number 1.96 is the value of the z-distribution ($z_{0.95/2}$) evaluated for a large dataset and a probability of 95%. The total uncertainty ($W_{\Delta T}$) can be calculated by taking the root mean square (rms) of the random uncertainty and the bias uncertainty ($B_{\Delta T}$) which is the result of the temperature sensors (see Eq. (3.8)). Note that these are absolute uncertainties with units of K. Throughout this chapter all uncertainties will be

written as absolute values, when a relative value is appropriate a fractional notation will be used.

$$W_{\Delta T} = \sqrt{\left(P_{\Delta T}{}^2 + B_{\Delta T}{}^2\right)} \ [K] \qquad (3.8)$$

where $B_{\Delta T}$ is taken as 0.05 K. The result of this calculation is a set of mean temperature drops between the sensors $\Delta T_{i \to j} \pm W_{\Delta T i \to j}$. These can then be used to calculate the temperature gradient in the meter bars using Eq. (3.3). The uncertainty is determined by taking the rms of the relative uncertainty associated with each of the values as follows:

$$\left(\frac{dT}{dz}\right)_{hot} = \left(\frac{\Delta T_{1 \to 3}}{d_{1 \to 3}}\right) \ \left[\frac{K}{m}\right] \pm \sqrt{\left(\left(\frac{W_{\Delta T_{1 \to 3}}}{\Delta T_{1 \to 3}}\right)^2 + \left(\frac{W_{d_{1 \to 3}}}{d_{1 \to 3}}\right)^2\right)} \ [\%] \qquad (3.9)$$

$$d_{1 \to 3} = (l_1 - l_3) \ [m] \pm \sqrt{U_{l_1}{}^2 + U_{l_3}{}^2} \ [m] \qquad (3.10)$$

Where the measurements l_1 and l_2 are the distance of the various probe holes from the interface as measured via CMD and U_l is the uncertainty in the CMD readings and is taken as 0.01 mm. The remaining terms in Eq. (3.1) can be calculated using the same method being sure to use the relative uncertainty when multiplying and the absolute uncertainty when doing a sum:

$$\frac{Q}{A} = k\left(\frac{dT}{dz}\right) \ \left[\frac{W}{m^2}\right] \pm \sqrt{\left(\left(\frac{W_k}{k}\right)^2 + \left(\frac{W_{(dT/dz)}}{\left(\frac{dT}{dz}\right)}\right)^2\right)} \ [\%] \qquad (3.11)$$

$$\Delta T_{H\to C} = (\Delta T_{3\to 4} - \Delta T_{3\to H} - \Delta T_{C\to 4})[K]$$

$$\pm \sqrt{\left(W_{\Delta T_{3\to 4}}\right)^2 + \left(W_{\Delta T_{3\to H}}\right)^2 + \left(W_{\Delta T_{C\to 4}}\right)^2}\ [K] \tag{3.12}$$

Where $\Delta T_{3\to H}$ and $\Delta T_{C\to 4}$ are calculated as follows:

$$\Delta T_{3\to H} = d_{3\to H} \left(\frac{dT}{dz}\right)_{hot} [K] \pm \sqrt{\left(\frac{W_{d_{3\to H}}}{d_{3\to H}}\right)^2 + \left(\frac{W_{(dT/dz)_{hot}}}{\left(\frac{dT}{dz}\right)_{hot}}\right)^2}\ [\%] \tag{3.13}$$

$$\Delta T_{C\to 4} = d_{C\to 4} \left(\frac{dT}{dz}\right)_{cold} [K] \pm \sqrt{\left(\frac{W_{d_{C\to 4}}}{d_{C\to 4}}\right)^2 + \left(\frac{W_{\left(\frac{dT}{dz}\right)_{cold}}}{\left(\frac{dT}{dz}\right)_{cold}}\right)^2}\ [\%] \tag{3.14}$$

Note the inclusion of an uncertainty for the thermal conductivity of the meter bars in Eq. (3.11). The typical conductivity value of 167 W/m·K for Al 6061 T6 was taken from the ASM Metals Handbook: Volume 2 but no information on the uncertainty of this value was found and therefore was not included in the results shown in chapter 4. Ideally the thermal conductivity of the meter bars would be measured and this would alleviate the need to rely on published values. (American Society for Metals, ASM International. Handbook Committee, 1990)

Ultimately, the interface conductance and the associated uncertainty can be calculated using the following equation.

$$\theta = \left(\frac{Q}{A}\right)(\Delta T_{H\to C})^{-1} \left[\frac{W}{m^2 K}\right] \pm \sqrt{\left(\frac{W_{(Q/A)}}{\left(\frac{Q}{A}\right)}\right)^2 + \left(\frac{W_{\Delta T_{H\to C}}}{\Delta T_{H\to C}}\right)^2}\ [\%] \tag{3.15}$$

The uncertainty in the conductance value now includes the random uncertainty associated with the temperature measurements and uncertainty associated with the temperature sensors and CMD.

Using the data set shown in Fig. 3.3, the following is an example of a conductance calculation.   Firstly, the average temperature differences: $\Delta T_{1\to3}$, $\Delta T_{3\to4}$, $\Delta T_{4\to6}$ are calculated from the raw data.

$$\Delta T_{1\to3} = 1.8169\ K \quad \Delta T_{3\to4} = 4.2927\ K \quad \Delta T_{4\to6} = 1.8603\ K$$

Using Eqs. (3.7) and (3.8) the uncertainty in these values can be calculated.

$$P_{\Delta T1\to3} = \frac{1.96 \times 0.0037}{\sqrt{2396}} = 1.48 \times 10^{-4}K$$

$$(3.16)$$

$$P_{\Delta T3\to4} = \frac{1.96 \times 0.0045}{\sqrt{2396}} = 1.80 \times 10^{-4}K \qquad (3.17)$$

$$P_{\Delta T4\to6} = \frac{1.96 \times 0.0038}{\sqrt{2396}} = 1.52 \times 10^{-4}K \qquad (3.18)$$

These calculations result in small values as a result of a small standard deviation and large sample size.

$$W_{\Delta T1\to3} = \sqrt{((1.48 \times 10^{-4})^2 + 0.05^2)} = 0.05\ K \qquad (3.19)$$

The much larger uncertainty associated with the RTD dominates the rms equation.

$$\Delta T_{1\to3} = 1.8169 \pm 0.05\ K \quad \Delta T_{3\to4} = 4.2927 \pm 0.05\ K \quad \Delta T_{4\to6} = 1.8603 \pm 0.05\ K$$

Initially, it seems concerning that the top temperature drop is smaller than the bottom but on closer inspection the difference is within the error bounds. Equation (3.9) is used to calculate the temperature gradient along the length of the meter bars.

$$\left(\frac{dT}{dz}\right)_{hot} = \left(\frac{1.8169}{0.02541}\right) \pm \sqrt{\left(\left(\frac{0.05}{1.8169}\right)^2 + \left(\frac{0.014}{25.41}\right)^2\right)} = 71.5033 \frac{K}{m} \pm 2.75\% \quad (3.20)$$

$$\left(\frac{dT}{dz}\right)_{cold} = \left(\frac{1.8603}{0.02542}\right) \pm \sqrt{\left(\left(\frac{0.05}{1.8603}\right)^2 + \left(\frac{0.014}{25.42}\right)^2\right)} = 73.1825 \frac{K}{m} \pm 2.69\% \quad (3.21)$$

Equations (3.12) to (3.14) are used to calculate the temperature drop across the interface.

$$\Delta T_{3 \to H} = 0.01262 \times 71.5033 \pm \sqrt{\left(\frac{0.014}{12.62}\right)^2 + (0.0275)^2} = 0.9021 \ K \pm 2.75\% \quad (3.22)$$

$$\Delta T_{C \to 4} = 0.01258 \times 73.1825 \pm \sqrt{\left(\frac{0.014}{12.58}\right)^2 + (0.0269)^2} = 0.9206 \ K \pm 2.69\% \quad (3.23)$$

$$\Delta T_{H \to C} = (4.2927 - 0.9206 - 0.9021) \pm \sqrt{(0.05)^2 + (0.025)^2 + (0.025)^2}$$
$$= 2.4700 \pm 0.06 \ K \quad (3.24)$$

Equation (3.11) is used to calculate the heat transfer through the interface.

$$\frac{Q}{A} = 167 \left(\frac{71.5033 + 73.1825}{2}\right) = 12081.2643 \left[\frac{W}{m^2}\right] \pm 2.72\% \quad (3.25)$$

Finally, the interface conductance can be calculated.

$$\theta = 12081.2643 \times (2.4700)^{-1} \pm \sqrt{(0.0272)^2 + \left(\frac{0.06}{2.47}\right)^2} = 4891 \left[\frac{W}{m^2 K}\right] \pm 3.67\% \quad (3.26)$$

$$\theta = 0.49 \left[\frac{W}{cm^2 K}\right] \pm 4\%$$

Note that four decimal places were kept throughout the calculation and then the appropriate significant digits were used at the end of the calculation so that values would line up better with the calculations carried out by the Matlab script.

CHAPTER 4: EXPERIMENTAL RESULTS

The results presented are calculated using the steady state assumptions as discussed in the previous chapter. Results are presented graphically showing the interface conductance as a function of the clamping pressure. Manufacturer values are also presented where they are available. Each of the points shown represents one set of temperature measurements.

4.1 Conductance Results for No TIM

The logical starting place for testing was conductance measurements of the test interface with no TIM applied. The results of these tests are shown in Fig. 4.1. Note that the third point in the third data set was used in the calculation example in Chapter 3.
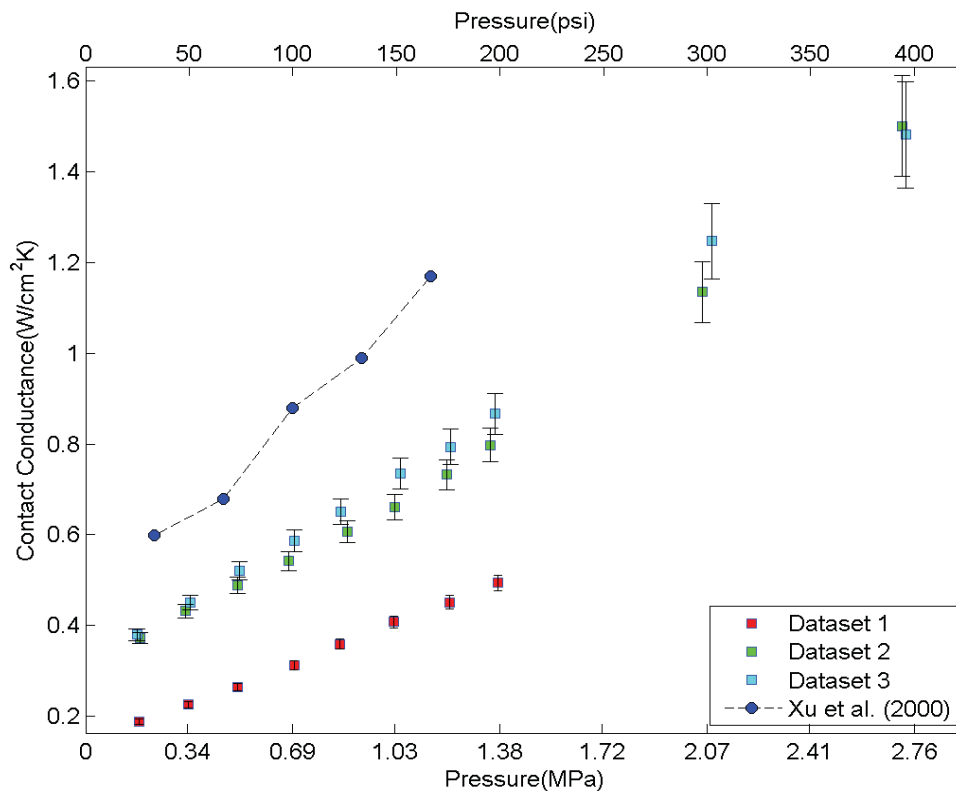

Figure 4.1 Conductance measurements of the bare interface (no TIM) assuming one dimensional heat flow.

The relationship between pressure and conductance appears linear in the case of no applied TIM within the pressure range tested. The data shown for comparison is taken from Xu et al. (2000) and was done using mechanically polished meter bars made of copper using the laser flash diffusivity method. The meters bars used in this thesis work were Al 6061 T6 machined to a #6 machine finish, not polished. This alone would account for the discrepancy in values. The difference in materials could potentially affect the conductance of the bare interface as well.

The first of the three dataset was measured just after the meter bars were machined. There is an approximately 0.2 W/cm^{2}K offset between this data set and the following two datasets. Datasets two and three were taken after the meter bars had been used for ~15 other test runs. This change in the contact conductance is more than likely the result of the deformation of the meter bar's surface features after the repeated application of pressure and elevated temperatures. It is also possible that there could have been contamination with TIM residue. However, the bars were carefully cleaned with acetone between each test and there does not appear to be any clear trend in the other experiments where later tests show higher conductance values. It would be helpful to investigate this further by imaging the surface characteristics at high magnification before and after testing to look for deformation and very small scale TIM residue trapped in micro scale features.

4.2 Conductance Results for Tgrease 880

Tgrease 880 is the only true grease or paste that was tested. All of the other materials were more similar to pads than to a liquid paste. It was applied generously to the face of one of the meter bars (see Fig. 4.2). Then when the two meter bars were put together and placed in the press under low pressure (< 0.14MPa or 20 psi) the majority of the applied TIM flowed out of the interface. The excess TIM was cleaned before testing. Figure 4.3 shows a photograph of the interface after the excess TIM was removed but before testing.

51

Figure 4.2 Photograph of a Tgrease 880 sample after being initially applied to the meter bar.
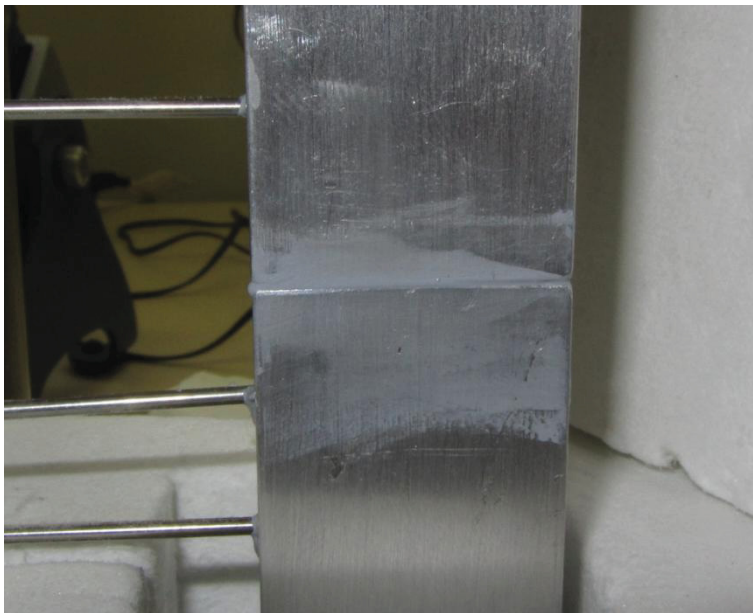

Figure 4.3 Photograph of a Tgrease 880 sample after being initially placed in the press and the excess TIM removed.

Figure 4.4 shows the conductance data that was measured. The trend show the conductance of the TIM increases linearly with pressure within the range tested. However, the uncertainties associated with the conductance measurements shown in Fig. 4.4 are high. This is a result of the high performance of the TIM and the heat flux applied during this test. The first set of testing on all TIMs was run at an input voltage of 40 V. At this voltage the experimental heaters produce approximately 10 W of power. This set point was selected in order to keep the maximum temperature around 70°C (this temperature varied depending on the TIM in question). Tgrease 880 has a much higher performance than any of the other selected TIMs and this resulted in a small temperature drop across the interface at 10 W. As a result the uncertainty in the temperature measurements was too high to properly determine the conductance. The second test was run at approximately 20 W and shows an improvement in the uncertainty. However, when running the experiment at 20 W the maximum temperature reached 100°C and this will have increased the bias associated with lateral heat loss.

Experimentally, the best way to improve the characterization of high performance samples like greases is to increase the cooling capacity of the setup. By increasing the cooling capacity the total heat flow through the sample can be increased while maintaining an average operating temperature which will control heat losses. This could be done by optimizing the heat sink design and increasing the velocity of the airflow or by switching to a liquid cooled system. A flow through heat exchanger running water through a chiller loop and through a small block heat exchanger is one potential option.
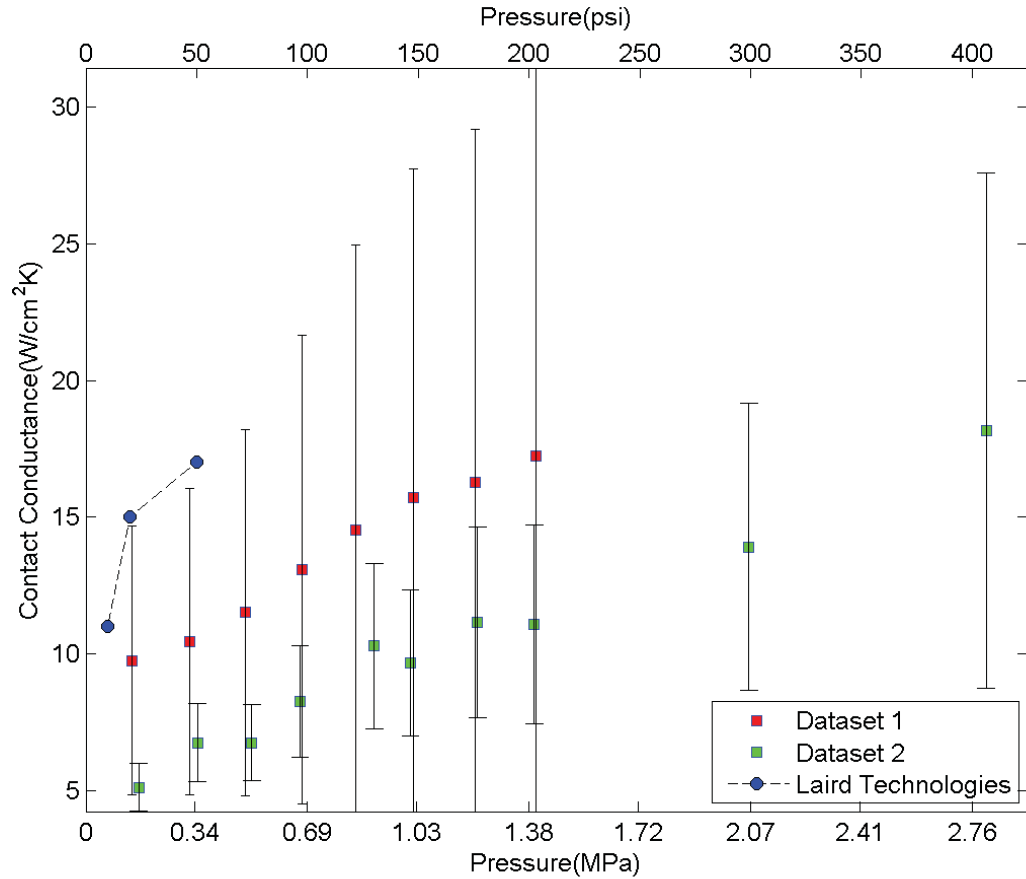
Figure 4.4 Conductance measurements of Tgrease 880 assuming one dimensional heat flow. (Laird Technologies, 2010a)

4.3 Conductance Results for Tflex 720

Tflex 720 is a soft pad TIM. A one inch square sample was cut and applied to the interface. It is quite tacky and this made it easy to assemble. When the TIM was placed in the interface the Tflex 720 quite effectively adhered to the two meter bars together helping with the alignment and handling of the test assembly. Figures 4.5 and 4.6 show a sample after a full test to 2.76 Mpa (400 psi). Tflex 720 was readily squeezed out of the interface. When the sample was removed from the test assembly it was not reusable. Figure 4.7 shows the measured conductance values for two runs of the experiment.

Figure 4.5 Photograph of a Tflex 720 sample after testing while still in the interface
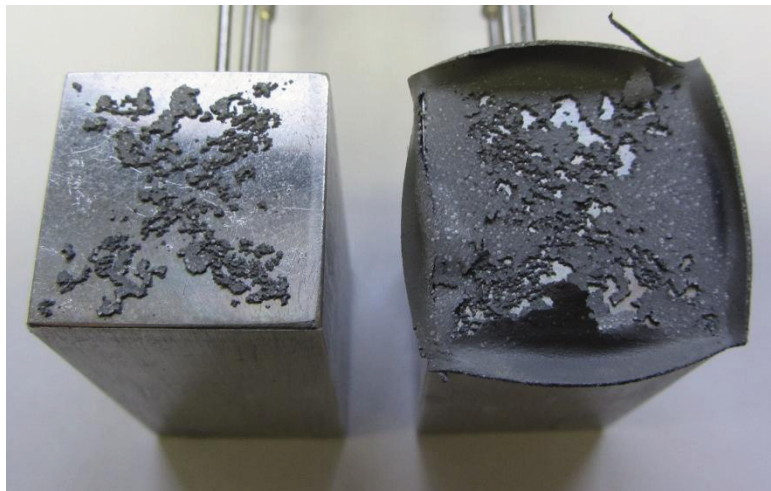
Figure 4.6 Photograph of a Tflex 720 sample after testing with the meter bars separated
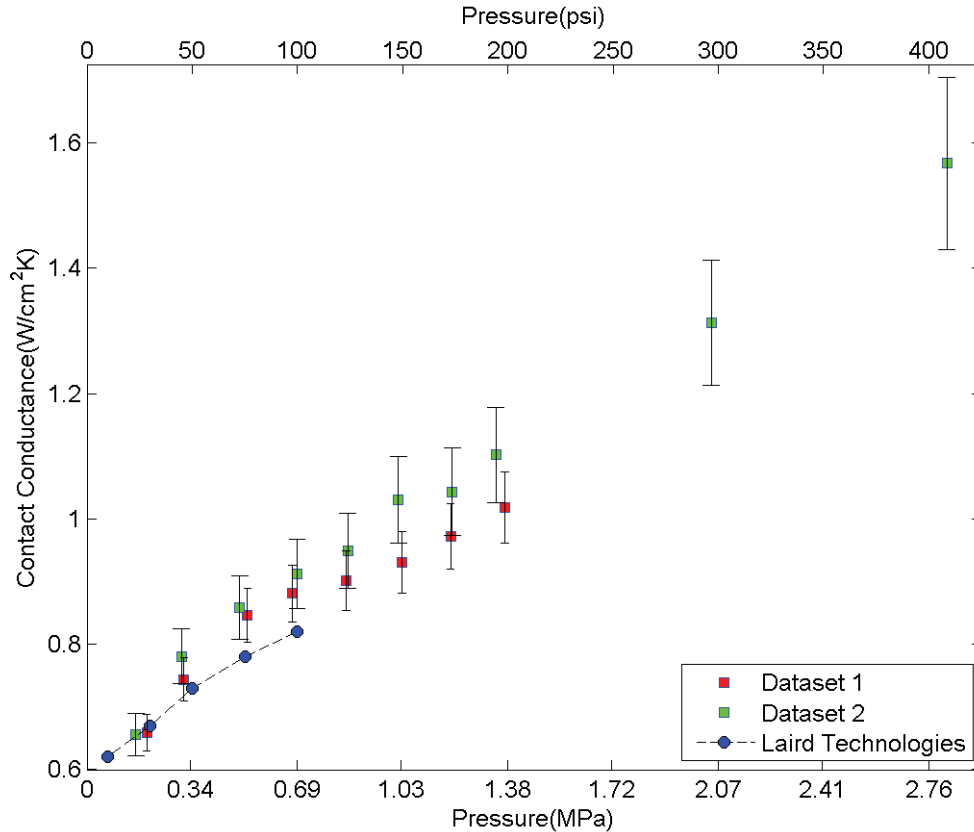
Figure 4.7 Conductance measurements of Tflex 720 assuming one dimensional heat flow. (I. Bryson, personal communication, June 11, 2012)

The overall trend appears linear within the range of clamping pressures tested. There is small variation between the two different runs especially between 1.03 and 1.38 MPa (150 and 200 psi). This is likely the result of how the pressure was applied. Significant amounts of Tflex 720 were squeezed out of the interface. As was discussed in the previous chapter the pressure relaxation problem made it somewhat imprecise to set and maintain a certain pressure. This could result in some variation in TIM thickness between tests. Also, variations in surface wetting and material composition could cause small difference between samples.

The measured values also correlate well with the supplied manufacturer data. The measured values seem to be trending slightly above the performance quoted by the manufacturer.

4.4 Conductance Results for Tmate 2905c

Tmate 2905c is unique among the tested TIMs as it consists of a phase change material adhered to a metal foil substrate. This means that one side of the interface will be in contact with the phase change material and the other will be in contact with the foil. As a result of the reinforcing foil the material is strong and easy to handle. During testing a considerable amount of the phase change material was squeezed out of the interface. Figure 4.9 shows a photograph of a sample of Tmate 2905c after a test sequence to 2.76 MPa (400 psi). Only a very thin layer of the phase change material remains on the foil after testing. Figure 4.8 presents the measured values of interface conductance for two samples of Tmate 2905c. Note, the first data set was measured with the PCM side facing down away from the heater and the second was measured with the PCM facing up.
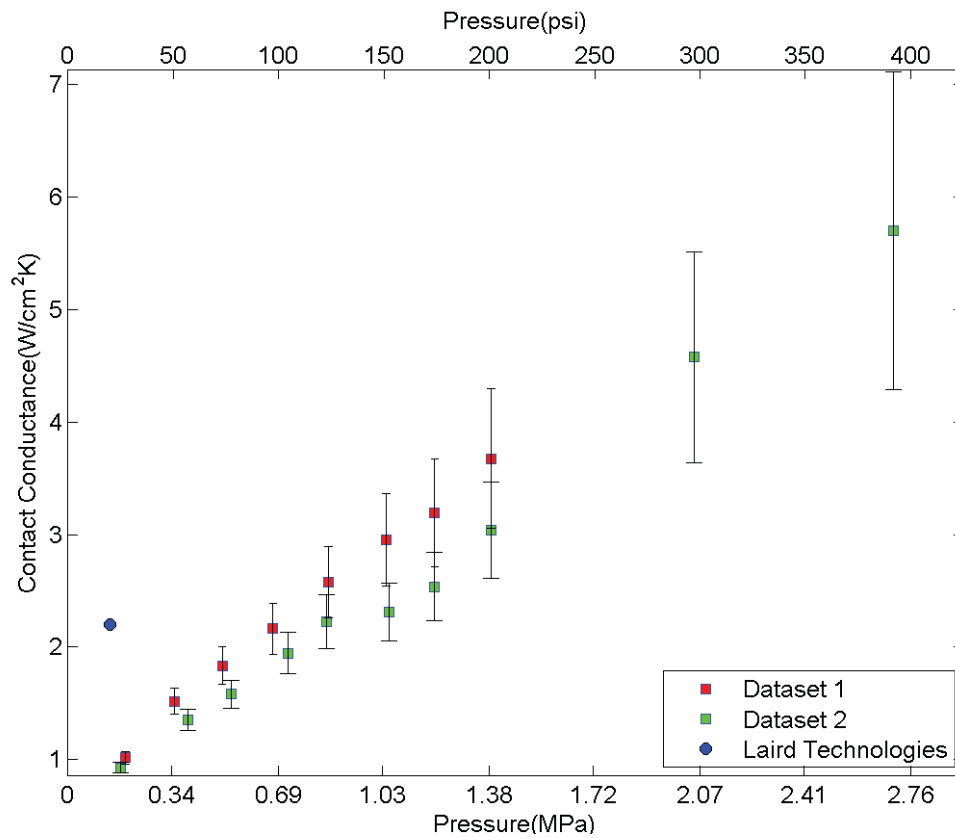
Figure 4.8 Conductance measurements of Tmate 2905c assuming one dimensional heat flow. (Laird Technologies, 2012)
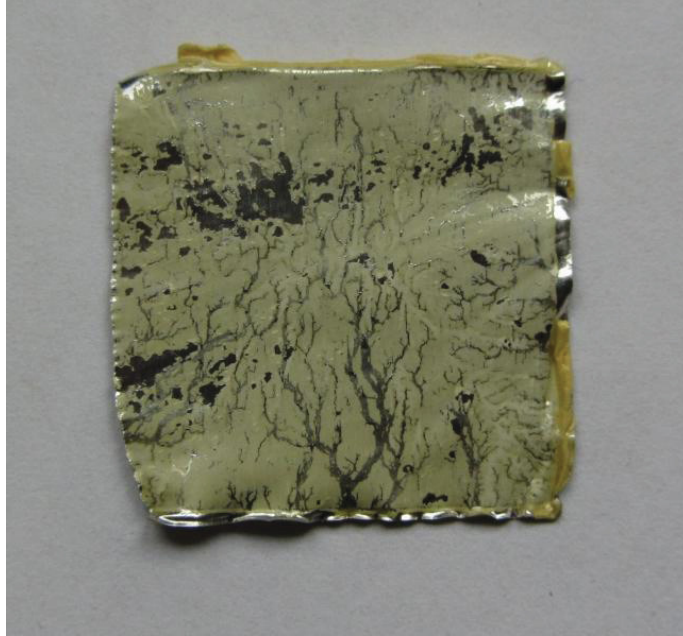
Figure 4.9 Photograph of a Tmate 2905c sample after testing

Once more the conductance values for the TIM appear to have a roughly linear relation with clamping pressure within the range of pressures tested. The measured value is in the same order of magnitude as the manufacturer published value. The measured value is lower by approximately 1 W/cm^2K. However, the surface characteristics of the test apparatus used by the manufacturer are not known. If they used polished surfaces on the apparatus it would be expected that the conductance would be lower with our test setup. A discrepancy due to differences in surface conductions would be more pronounced at lower pressures and with materials which conform poorly to surface features. In the case of Tmate 2905c, the foil side of the TIM could be increasing the significance of the surface finish. The only way to gauge this importance would be to retest the sample using meter bars with a different roughness. This will be discussed further in the future work portion of this thesis.

4.5 Conductance Results for Tpcm HP105

Tpcm HP105 is a white pad material when at room temperature. It was somewhat difficult to handle because it was relatively easy to crack the material. Unlike Tmate 2905c, the Tpcm HP105 does not have any reinforcing material and it consists solely of a thin piece of phase change material. The technical specification sheet for the material says it should be tacky. The material that was tested was not tacky and was actually quite hard and brittle. This could be an indication that the material had dried out while being stored. The material has a one year shelf life and would have been approaching that at the time of testing. Figure 4.10 shows the measured conductance values for this material.

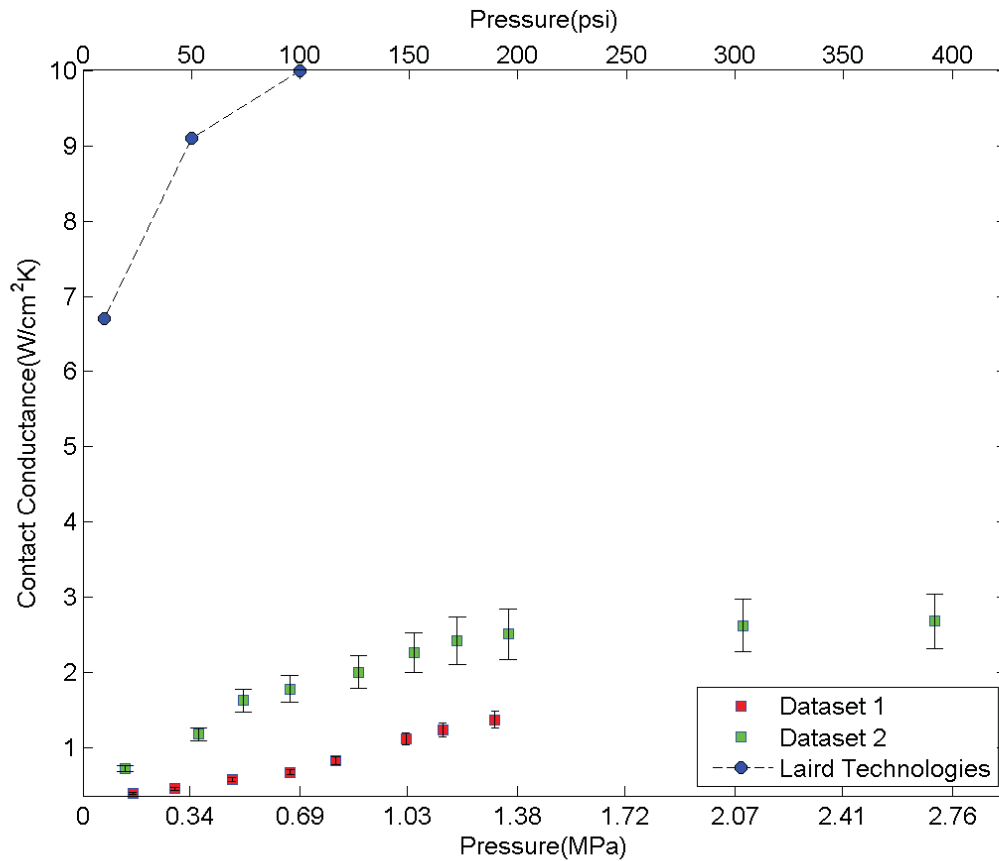**Figure 4.10 Conductance measurements of Tpcm HP105 assuming one dimensional heat flow. (Laird Technologies, 2010b)**

The relationship with pressure loading does not appear linear as with previous test cases. The increase in conductance levels off considerably after 1.38 MPa (200 psi). The materials performance was very poor in comparison with the conductance values published by the manufacturer. The first data set is more than an order of magnitude lower at 0.69 MPa (100 psi) of clamping pressure. This adds weight to the theory that the material degraded during storage. To investigate this further, the second sample was cut from the centre of a sample pad whereas the first sample was cut from the edge. There was a noticeable improvement in handling characteristics with the second sample, it was more flexible and less likely to crack. The conductance performance of the second sample was better than the first. There is a fair amount of evidence supporting the theory that the material may have degraded before testing. Further testing with a different batch of samples is needed before conclusions are made about the performance of Tpcm HP105. It is however interesting to see how much of an impact the age of the sample may have on the performance.

4.6 Conductance Results for Cho-Therm 1671

Cho-Therm 1671 is a reinforced elastomer pad. It is not tacky or adhesive and is much tougher than the Laird Technologies products discussed earlier in the chapter. There was no visual change in the sample before or after testing. Figure 4.11 shows a photograph of a sample of Cho-Therm 1671 after testing to 2.76 MPa (400 psi). Figure 4.12 presents the conductance measurements that were made.

Figure 4.11 Photograph of a Cho-Therm 1671 sample after testing
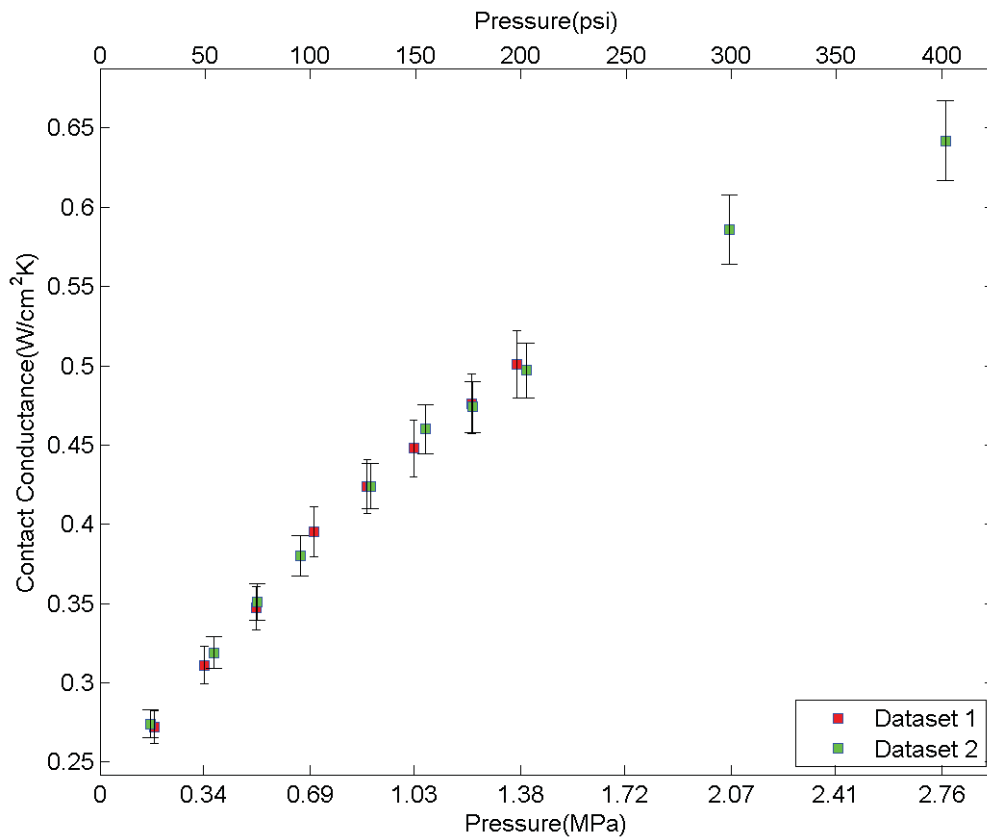
Figure 4.12 Conductance measurements of Cho-Therm 1671 assuming one dimensional heat flow. (Chomerics, 2001)

Cho-Therm 1671 tests showed a nonlinear relation between interface conductance and pressure. The conductance is approaching an asymptote; it is rising with increasing pressure to a maximum value. At higher pressures it does approach the manufacturer published interface conductance value of 0.676 W/cm^2K. Chomerics did not quote a clamping pressure at which the published conductance value was tested. However, the specification sheet does indicate that Cho-Therm 1671 is best used between 2.07 and 3.45 MPa (300 and 500 psi).

4.7 Conductance Results for Cho-Therm T500

Cho-Therm T500 is a reinforced elastomer pad which is very similar to Cho-Therm 1671. It is not tacky or adhesive and is much tougher than the Laird Technologies products discussed earlier in the chapter. There was no visual change in the sample before or after testing. Figure 4.13 shows a photograph of a sample of Cho-Therm 1671 after testing to 2.76 MPa (400 psi). Figure 4.14 presents the conductance measurements that were made.
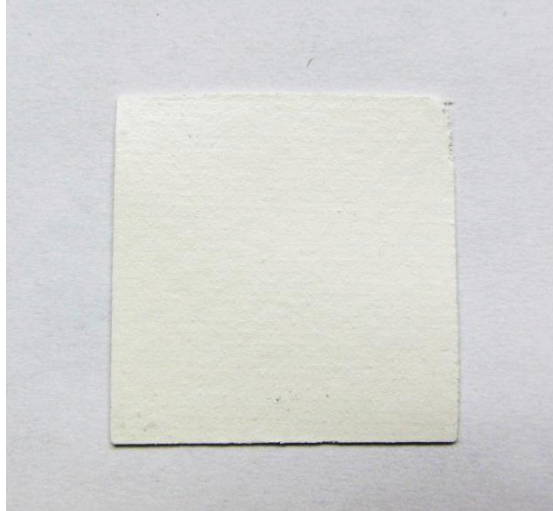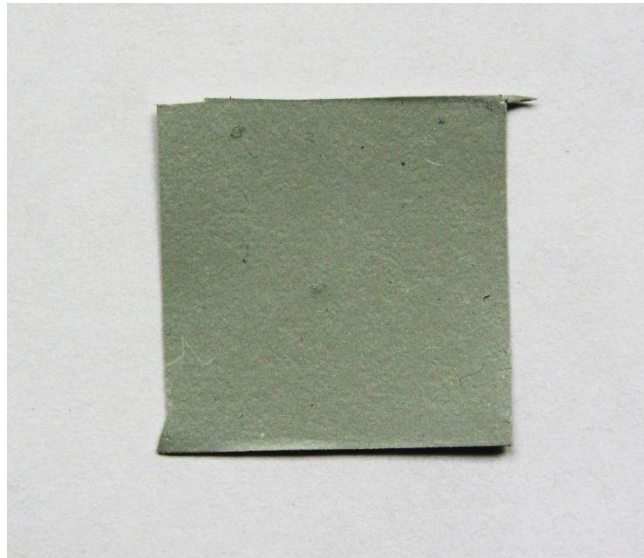

**Figure 4.13 Photograph of a Cho-Therm T500 sample after testing**
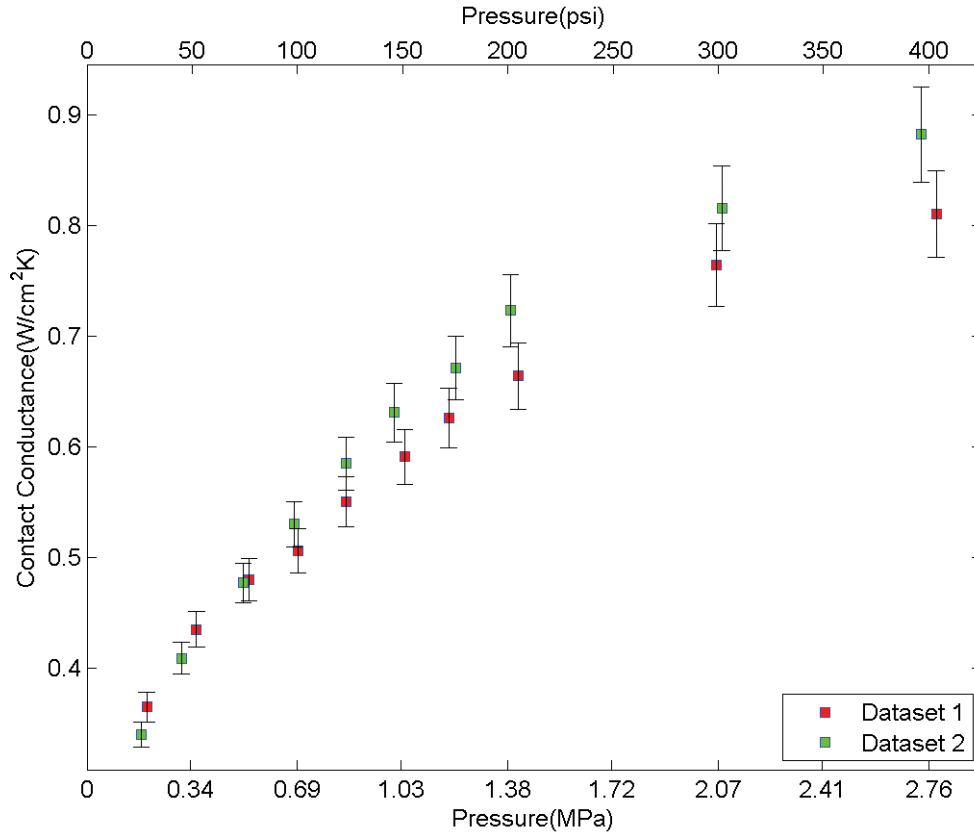
Figure 4.14 Conductance measurements of Cho-Therm T500 assuming one dimensional heat flow. (Chomerics, 1999)

Cho-Therm T500 shows similar nonlinear pressure dependence to Cho-Therm 1671. It is approaching an asymptotic maximum conductance as the clamping pressure is increased. The conductance is close to the conductance value, 0.813 W/cm^2/K, published by Chomerics at higher pressures.

63

4.8 Summary of Conductance Measurements

The measured conductance values for all of the materials excluding Tgrease 880 are summarized in Fig. 4.15. The Tgrease 880 values were excluded because of the large uncertainty associated with them. The majority of the TIMs did not exceed 1.5 W/cm^{2}K with the exception of Tmate 2905C and Tpcm Hp105. One thing to note is the conductance values of the Chomerics products. They are comparable or worse than the conductance of the interface with no TIM applied. This initially seems surprising, however, both of the Chomerics materials have additional design criterion in addition to being a TIM. They are both designed to electrically isolate the surfaces of the interface from one and other. Also, the designs of both materials had a strong focus on being rugged and reusable and are highly reinforced. Therefore, the comparison to the interface with no TIM is not as important a comparison as it is with the materials designed for the sole purpose of improving interface conductance.

Figure 4.15 Summary of all measured conductance values excluding Tgrease 880

CHAPTER 5: CALCULATION OF CONTACT CONDUCTANCE BY COMPARISON WITH A FEA MODEL

The one dimensional assumption used in the previous two chapters is a widely used method and simplifies the calculation of the interface conductance. However, any heat losses or non-unif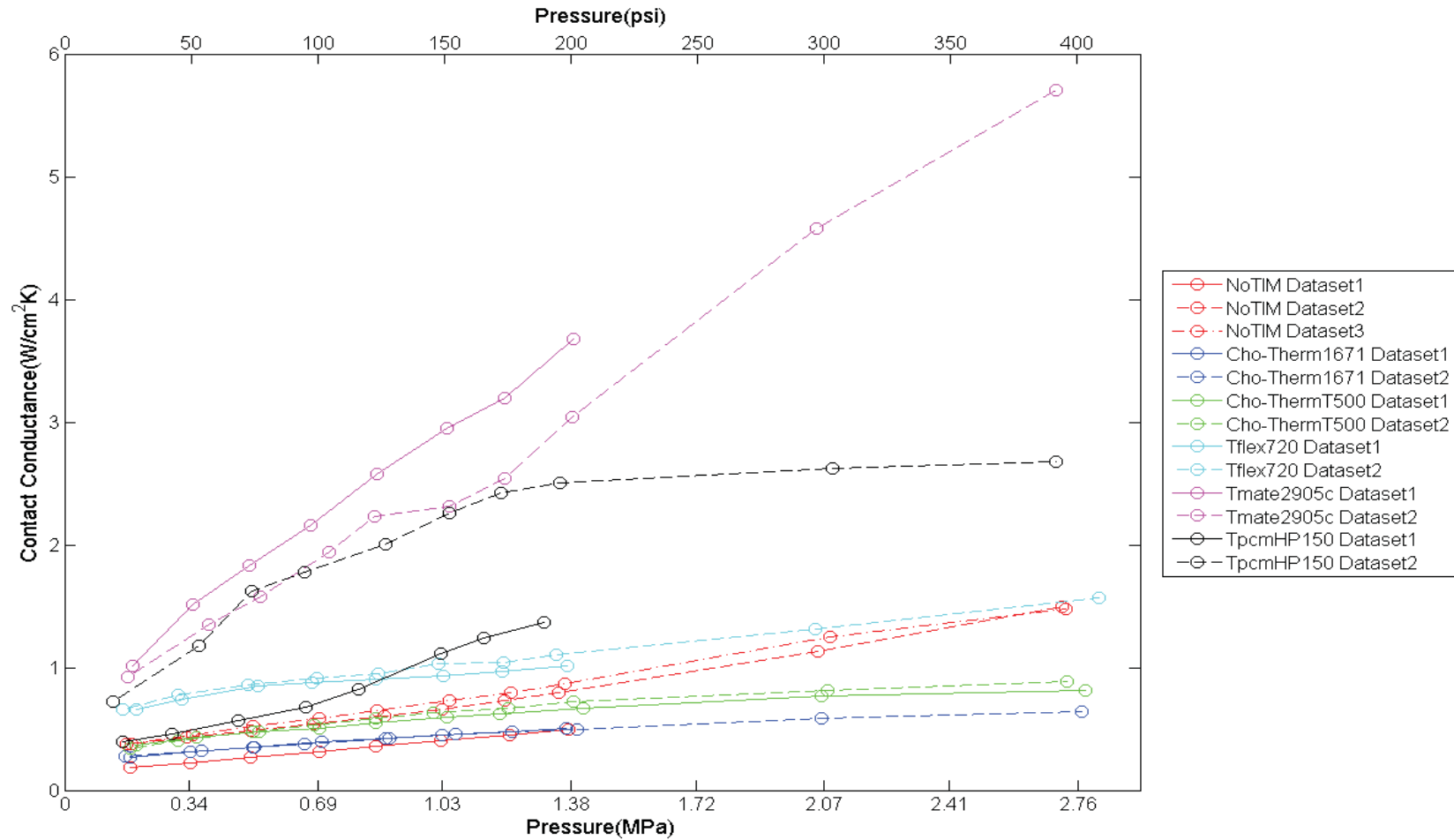ormity in the heat flux through the meter bars could introduce a bias into the experiment. At low experimental temperatures the heat losses are relatively small and the assumptions made in the above chapters are likely valid. However, in some cases, such as Tgrease 880, the performance of the TIM is high enough that the power through the test assembly must be increased in order to force a larger temperature drop across the interface. Increasing power will increase the average temperature of the test assembly and subsequently increase the heat losses unless the cooling rate could be increased as is further discussed in Chapter 6. A more complete model of the heat transfer could account for the heat losses associated with higher temperature testing. A more complete model would also foster a better understanding of the experiment as a whole which is a major goal of this thesis work. The first step in developing a more complete model was taken by creating a finite element analysis (FEA) model of the test assembly using COMSOL Multiphyisics 4.2a. This model was used to simulate the same data point shown in chapter 3 (no TIM at 0.50 MPa or 73 psi). This data point has already been discussed and has low uncertainty which makes it a good candidate for explaining the model and doing an initial verification between the model and experimental data.

5.1 Model Description

A three dimensional model of the assembly was created. Half of the setup was modeled; it was cut along the line of symmetry between the two heater cartridges which make up the test heater (see Fig. 5.1).
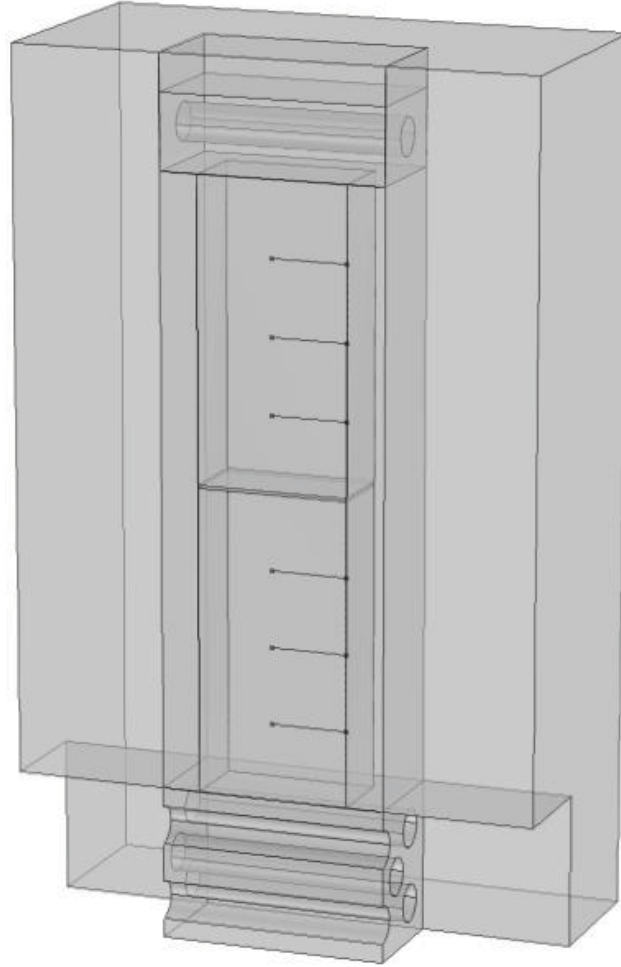
Figure 5.1: Geometry of FEA model of the experimental setup

All of the boundary conditions in the model were set as convection to an ambient temperature of 25 ºC except for the top of the Macor insulation which was set to be insulated to simulate the guard heater. All of the heat transfer within the test assembly model is by conduction. No convection within the air gap between the meter bars and the insulation was modeled because the heater will heat the air from the top. The hottest air will be at the top of the gap and no stable convection current will form. Three different heat transfer coefficients were used: $h_{lateralheatloss}$, $h_{heatsink}$, $h_{topheatloss}$. $h_{lateralheatloss}$ is the heat transfer coefficients associated with the outside vertical walls of the insulation jacket and $h_{heatsink}$ is the heat transfer coefficient at the surface of the heat exchanger. $h_{topheatloss}$ is the

heat transfer coefficient associated with the top of the insulation jacket. A separate coefficient for the top was assigned because it was observed that the profile in the meter bars was very linear indicating little heat loss through the sides of the assembly, however, 10.7W were input to the heater and the measured heat transfer through the assembly was 7.8W. Heat is being lost before it can conduct into the meter bars. This model simulates this heat loss with the boundary at the top of the insulating jacket.

RTDs are not point probes. The specific sensors used in the experimental setup had an element which was 0.5 inches (1.27 cm) long. In order to derive comparable values from the simulation the average temperature was taken along 0.5 inch lines located at the same locations as the sensors were in the actual experiment. These virtual sensor values will be used to compare to the experimental values.

The TIM layer was simulated by placing a thin domain between the meter bars and then assigning its thermal conductivity so that the thermal conductance of the layer would equal the conductance of the actual TIM interface (see Eq. 5.1).

$$k_{TIMdomain} = d_{TIMdomain} \times \theta \tag{5.1}$$

The conductance of a TIM can be simulated without having to simulate the actual thickness of the layer. This assumes that the edge effects associated with the thin domain are negligible. We can test the validity of this assumption by running several different simulations and checking to see how the solution changes. Figure 5.2 shows six consecutive tests with a TIM domain thickness of 0.125 mm to 4 mm doubling the thickness each step. Each of the plot lines represents the temperature measured at the locations of one of the experimental sensors. Figure 5.3 shows the same results but as the key temperature differences between virtual sensors.
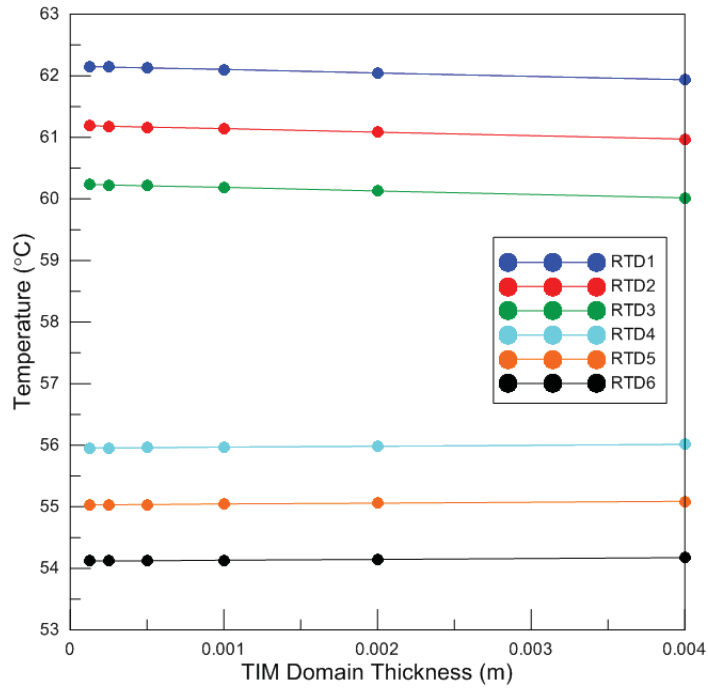
Figure 5.2 Analysis of the sensitivity of the simulation to the TIM domain thickness virtual sensor values
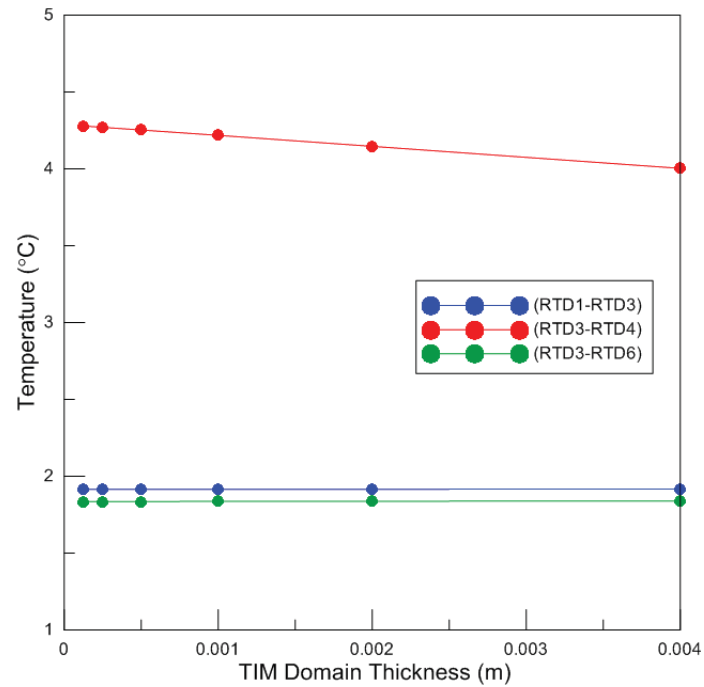
Figure 5.3 Analysis of the sensitivity of the simulation to the TIM domain thickness key temperature differences

The thickness of the TIM domain has only a weak effect on the results of the simulation once the thickness of the domain is small; a value of 0.5 mm was used for the remainder of the simulations.

5.2 Mesh and Convergence

The model was meshed using tetrahedral elements. It was meshed in two sections. The core section, consisting of: the meter bars, heater, heat sink and air gap was meshed using relatively small elements as this is where the majority of heat transfer happens. The outer insulating jacket was meshed using relatively large elements as little heat transfer happens in this domain. A convergence study was done varying the maximum size of elements in each of these sections.

Figure 5.4 shows the results from the convergence study done on the outer insulation domain. The maximum element size was varied from 0.00375 m to 0.06 m doubling the element size each time (maximum element size is defined as the longest side of an individual element). The maximum element size, in the insulation domain, has little effect on the solution; 0.015 m was used in the simulations in section 5.1 and 5.3.
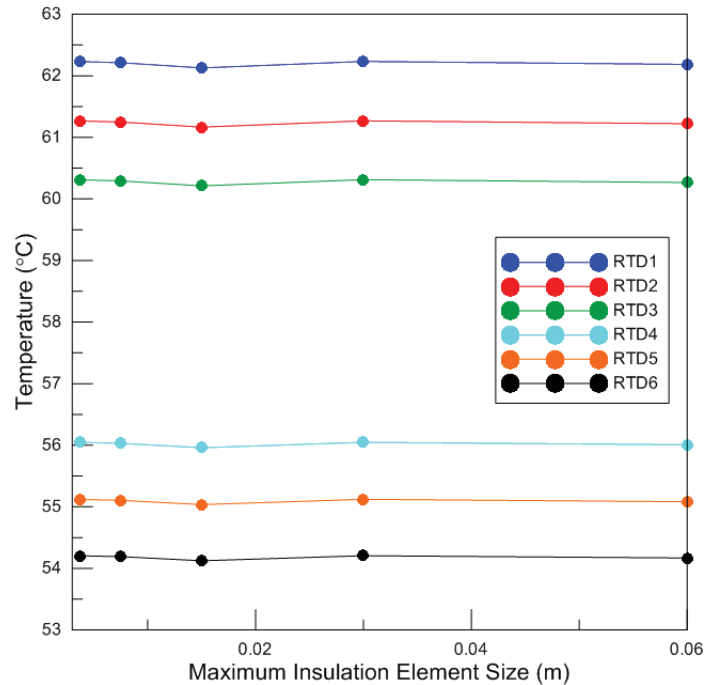
Figure 5.4 Convergence study for the insulation domain mesh

Figure 5.5 shows that there is still work to be done with this simulation. The maximum core element size was varied from 0.001 m to 0.032 m doubling the element size on each step. Oddly, the trend starts out linear and then starts to increase as the elements get smaller. We have a diverging mesh, the element size chosen for the simulations was 0.002 m. The next logical step for this analysis would be to move to a more powerful computer and extend this analysis to smaller elements to see if the trend levels off. Also, the different domains currently meshed together could be meshed and analyzed separately. Given access to a more advanced meshing program a square mesh could be used or perhaps a hybrid mesh with some components meshed in square elements and others in tetrahedral elements. Figure 5.6 shows the mesh used in the simulations presented in section 5.1 and 5.3.
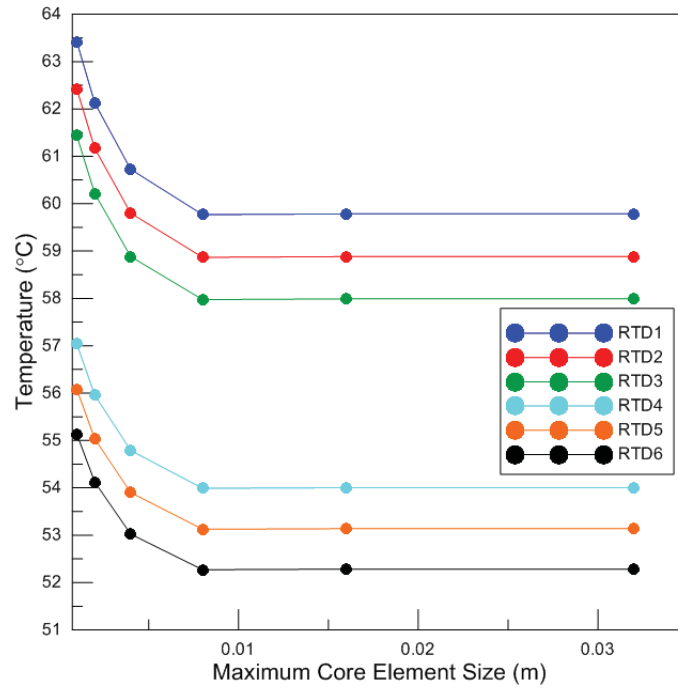
Figure 5.5 Convergence study for the core domain mesh
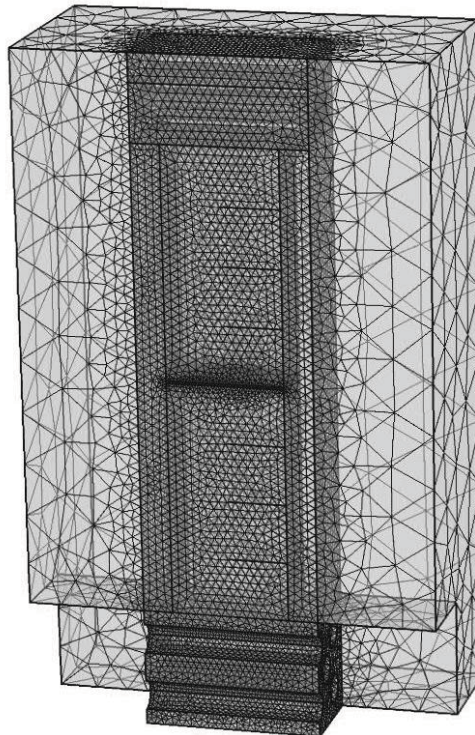
Figure 5.6 Mesh used to discretize the model

5.3 Comparison with Experimental Results

The values of the three heat transfer coefficients defined in section 5.1 were used to fit the FEA model to the experimental results for no TIM at 0.50 MPa (73psi) (this is the same data point which was detailed in Chapter 3). The heat transfer coefficients used are shown in Table 5.1. It should be noted that the heat transfer coefficient of the heat loss out of the top of the model is a somewhat artificial perimeter used to simulate the heat loss out of the top of the experimental setup, not an approximation of a real convective coefficient.

Table 5.1 Summary of the heat transfer coefficients used in the simulation

$h_{lateralheatloss}$	5 W/m²K
$h_{heatsink}$	44.4 W/m²K
$h_{topheatloss}$	2600 W/m²K

Figures 5.7 and 5.8 compare the virtual sensor temperatures and key temperature differences produced by simulation to the experimental results. The temperatures all match up within the uncertainty of the experimental values and the temperature differences match up well. There is a bit more heat losses in the simulation than was seen in the experiment, the heat loss coefficients could possibly have been fitted better. These coefficients were manually fitted to the data. It would be an interesting extension of this work to use a least squares approach to the fitting process. This could be done efficiently by using the interface between MatLab and COMSOL 4.2a. For this fit of the data the conductance of the interface was found to be 0.5 W/cm²K very close to the value calculated with the one dimensional assumption: 0.49 W/cm²K.
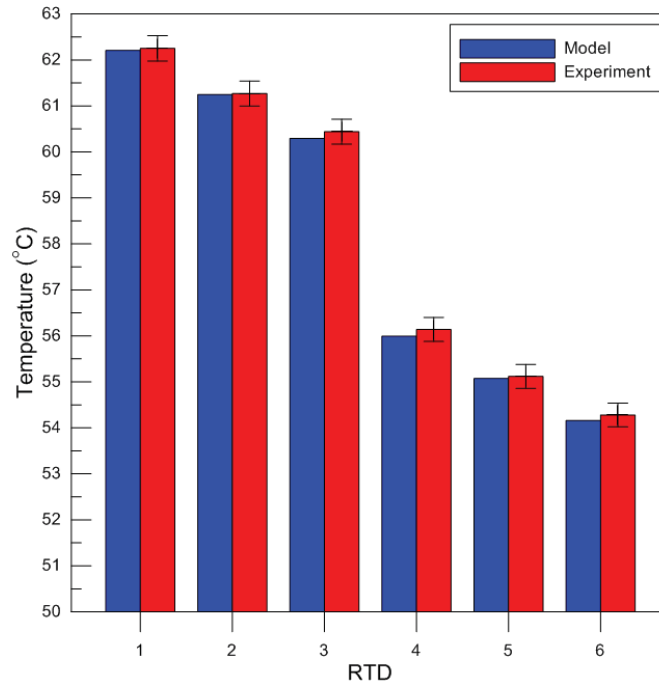
Figure 5.7 Comparison of the temperature produced by the FEA model and the experimental setup
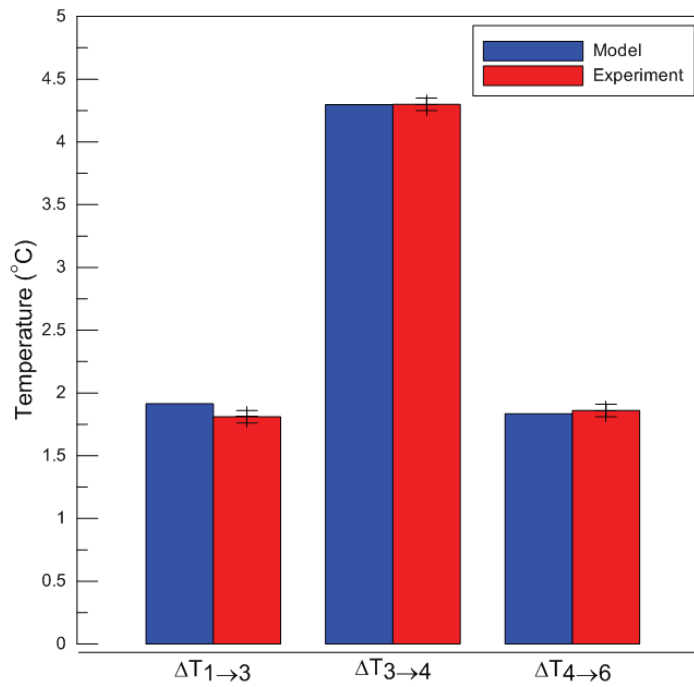
Figure 5.8 Comparison of the key temperature differences produced by the FEA model and the experimental setup

Figure 5.9 shows a plot of the temperature profile, from the simulation, along a line going up the centre of the meter bars. It shows, that with this fit to the data, the simulated setup is operating close to a one dimensional system. The temperature change through the meter bars is linear and a well-defined jump through the TIM layer can be seen.
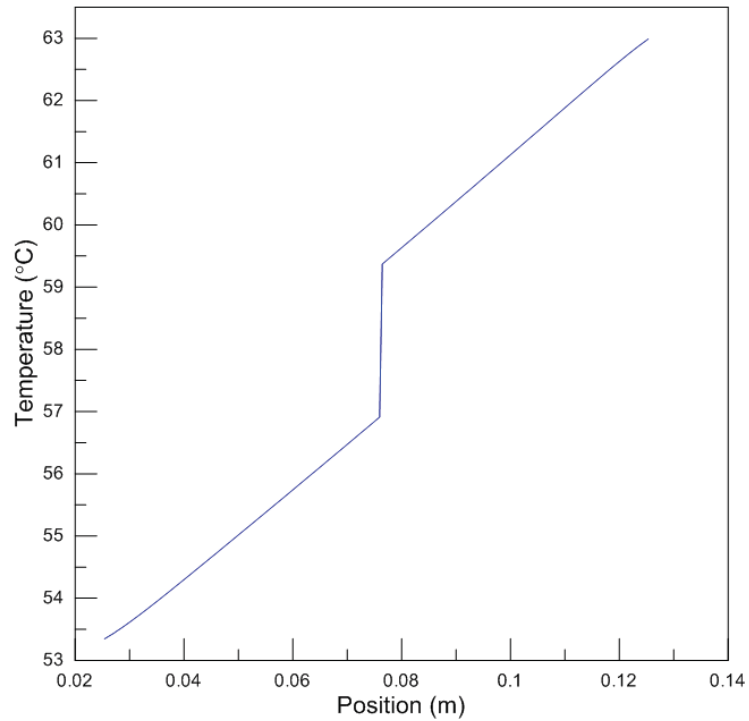
Figure 5.9 Temperature profile along the centre line of the meter bars from the FEA simulation

Figure 5.10 is a graphical output from the simulation when using the coefficient fit described above. The colour scale represents isothermal surfaces and the arrows show the direction and magnitude of the heat transfer.
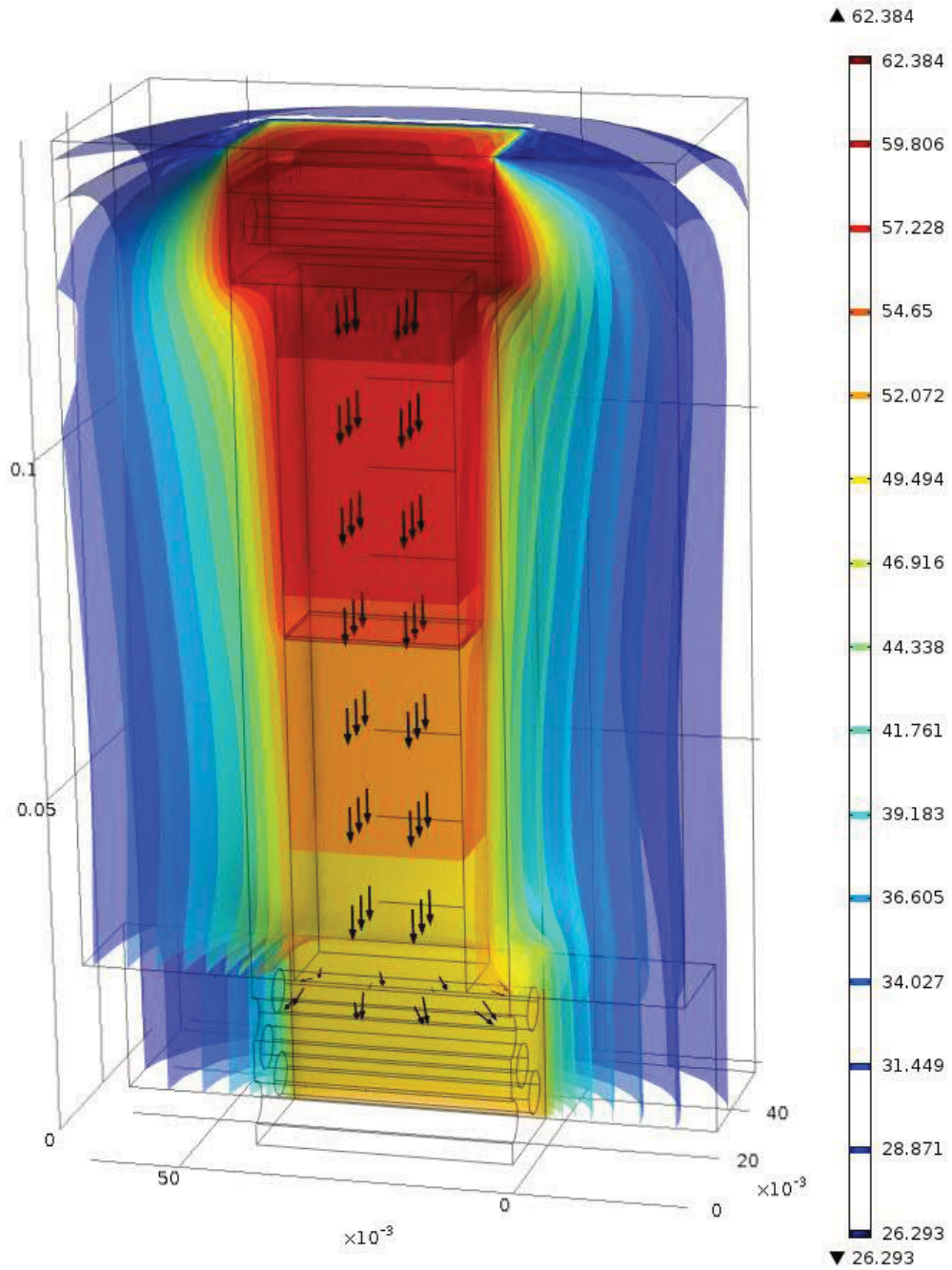
Figure 5.10 Graphical output from the simulation showing isothermal surfaces and arrows indicating the direction and magnitude of heat transfer

5.4 FEA Model Concluding Remarks

A preliminary FEA model of the experimental setup was created using COMSOL Multiphysics 4.2a. The model was a three dimensional simulation of half of the setup cut down the line of symmetry between the cartridge heaters. Three heat transfer coefficients were used to fit the model to a single experimental data point (no TIM at 0.50 MPa (73psi)). It was shown that when this method of manual fitting was used the model gave very similar results to the experimental setup, including predicting the conductance value of the TIM. For this particular dataset and fitting parameters the model is very successful. However, the mesh is not converged. These results are promising but work must be done to improve the mesh before this simulation can be extended to other circumstances. It would also be advantageous to use a least squares approach to fitting the heat transfer coefficients instead of manually fitting the values.

The next step will be to expand the number of data points modelled and attempt to compare the data collected during a high temperature run where heat losses are more important. The model is useful for better visualizing the physics associated with the experimental apparatus.

CHAPTER 6: CONCLUSIONS AND FUTURE WORK

6.1 Concluding Remarks

A steady state interface conductance characterization device was designed and built. This device was designed to establish a one dimensional heat flow through a sample of TIM which is held in a test interface between two aluminum meter bars. A methodology for measuring the interface conductance of TIMs as a function of clamping pressure was developed.

The interface conductance of the bare interface with no TIM and six different commercial TIM materials were tested using the steady state characterization method. Conductance values were measured at clamping pressures between 0.17-2.76 MPa (25-400 psi). The materials tested were: Tgrease 880, Tflex 720, Tmate 2905c, Tpcm HP105, Cho-Therm 1671, and Cho-Therm T500. The first four of these materials were TIMs sold by Laird Technologies and the last two from Chomerics.

It was found that the conductance of the bare interface trended up linearly with increasing clamping pressure over the range of pressures tested. The measurements showed that the conductance of the bare interface increased by nearly a factor of two from the first test to the second test. For comparison, just after it was machined the bare interface was measured to have an interface conductance of 0.19 W/cm^2K and 0.49 W/cm^2K at 0.18 and 1.37 MPa (26 and 199 psi) respectively. After approximately 15 test runs the interface conductance was measure to be: 0.38 W/cm^2K and 0.87 W/cm^2K at 0.17 and 1.37 MPa (25 and 198 psi) respectively. The reason for this increase is not known, but some combination of three possibilities is suspected. The repeated application of pressure to the test interface could have caused a permanent change to the surface characteristics increasing the conductance of the later tests. There could be microscopic TIM residue stuck in the surface features that was not removed by repeated cleaning.

Finally, it is possible there was a problem with the test procedure for the first dataset, for instance there could have been foreign debris in the interface causing a lowered conductance value. It would be an interesting extension of this work to image the surfaces at high magnification before and after testing to look for evidence for either changes in the surface features or TIM residue.

The results for the Laird Technologies products were varied. The measured results for Tflex 720 coincided well with the publish manufacturer data. The measured conductances for Tmate 2905c was in the same order of magnitude as the manufacturer published data but was offset approximately 1 W/cm^{2}K lower. Tpcm HP105 was measured to have a much lower performance than was published by the manufacturer. The measured values were more than an order of magnitude lower in some cases. There was evidence that the sample tested could have degraded during storage. Based on the very low performance and the fact that there was a change in physical properties and conductance between samples taken from the outer edge and centre of the stock sheet the author believes that further tests using a different supply of material is warranted. The final Laird Technologies product Tgrease 880 was problematic and highlighted one of the major improvements that could be made to the experimental setup. As a result of the greases relatively high performance when compared with the other TIMs tested the temperature drop across the interface was comparatively small. This small temperature drop resulted in a high uncertainty mainly due to the uncertainty associated with the RTDs. When the power applied to the setup was increased the uncertainty improved but more work needs to be done to improve the experimental setups ability to characterize high performance TIMs. The results for the two Chomerics products, Cho-Therm 1671 and Cho-Therm T500, matched well with manufacturer values under clamping pressures of 2.07-2.76 MPa (300-400 psi). The performance of these materials was pressure dependant and degraded by more than half when tested at 0.17 MPa (25 psi).

The interface conductance showed a linear trend with clamping pressure for the case of a bare interface and the Laird products excluding Tpcm HP105. For these cases it is likely that further increasing the pressure will improve the conductance of the interface. It

would be a useful extension of this work to test at pressures higher than 2.76 MPa (400 psi) to see how far the liner trend continues. In the case of Tpcm HP105 and the Chomerics products the rate of increase levels off and seems to be approaching a maximum conductance value. Further increasing the clamping pressure past 400 psi will provide much less gain in conductance for these materials.

A preliminary FEA model of the experimental setup was created in COMSOL Multiphysics 4.2a. The model was fitted to a set of experimental results using three heat transfer coefficients. The interface conductance was found to be 0.5 W/cm^2K using this model. This value correlates well with the experimental value calculated using the one dimensional assumption (0.49 W/cm^2K). The next step will be to model additional experimental data and improve the model with better meshing and an improved fitting methodology.

6.2 Future Work

There are a number of avenues for expanding on the work presented in this thesis. Some obvious improvements could be made to the experimental apparatus to expand its ability to characterize higher performance TIMs as well as improve its ease of use and repeatability. Also, there are opportunities for expanding the premise of the experiment. It would be interesting and useful to further expand the range of clamping pressures and to investigate the effect of temperature on the performance of TIMs. Investigation of the effect of surface roughness on conductance would also be a logical extension of this work.

The most impactful improvement which could be made to the TIM test apparatus would be an upgrade to the cooling system. Currently the system uses a custom built heat exchanger and a small computer fan to cool the system. This is sufficient for lower performance TIMs. However, as the performance increases the temperature drop across the interface becomes small and the uncertainty in the measured conductance increases. The best solution to this problem is to increase the power supplied by the heater. The more heat that is conducted through the interface the larger the temperature drop. The

current heater is rated for 100 W at 120VAC and the maximum heater power used in the tests presented in this thesis was 20 W. There is plenty of heating capacity in the current design to allow for an increase in power. However, there is not sufficient cooling power to maintain an acceptable average operating temperature with a higher power input. The maximum system temperature when operating at 20W was slightly more than 100 ºC. With temperatures much higher than the ambient, lateral heat losses become more likely. One potential solution to this problem would be the use of a liquid cooled system. An aluminum block heat exchanger coupled with a chilled liquid bath is one potential option. However, this discussion ties into the discussion of testing samples at a variable average temperature.

A second recommended improvement to the current design would be to upgrade the pressure application system. Currently, a simple screw press is used to manually apply a pressure to the assembly. However, it would be a considerable improvement to automate the pressure application. An automated press with a control circuit linked to the pressure sensor would allow the system to dynamically maintain a selected clamping pressure. This would improve repeatability by removing the need to readjust the press if there is an outflow of TIM or a change in average temperature. Automated pressure control also ties into the discussion of characterizing conductance at variable temperatures.

The simplest way to extend the scope of this work would be to increase the range of clamping pressures. Many of the materials tested showed a linear trend with increasing clamping pressure. This indicates that if the pressure was further increased the conductance would continue to increase. However, some of the TIMs approached a maximum conductance as the clamping pressure was increased. It is logical to posit that all TIMs would eventually reach a point where they no longer make additional gains from increased clamping pressure. Investigating where this limit is for each material and how their material properties affect this limit would be interesting.

Another logical extension of this work would be to repeat the same test procedure but with different surface features on the meter bars. The system was designed for the meter

bars to be easily removable to expedite their cleaning. It would be straight forward to produce a number of different meter bars with different surface features. Perhaps, a set with a courser finish and a set polished to a mirror finish.

Finally, this work could be extended to include the ability to test the interface conductance of samples at a variety of pressures and temperatures using the steady state method. This would entail being able to control the average temperature of the test assembly in addition to the clamping pressure. The average temperature of the assembly can be controlled by controlling the rate of cooling. If the system had a cooling system that could be readily modulated (for example a liquid cooling system where the coolant temperature and flow rate were controlled)   you could modulate the average temperature of the test assembly, and therefore the TIM, within a certain range. The upper limit of the range would be defined by the heat losses from the system and the lower limit would be defined by the ambient temperature and the coolant system. With the right setup you could potentially get good control over a limited range. Another option would be to optimize the heat sink cooling design instead of switching to liquid cooling and then place the whole test assembly in an environmental chamber. By modulating the temperature of the environmental chamber you could vary the operating temperature of the test assembly. The test assembly would continue to operate as before, reaching a steady state temperature 20 to 50 ºC above ambient but you would now control the ambient temperature. This would effectively remove the heat losses as a limit to the maximum test temperature it would now be limited by the environmental chambers maximum temperature. Using this method you could potentially modulate the average temperature from below zero to hundreds of degrees Celsius. There would be two main challenges to using this approach. Firstly, the test assembly would be inaccessible during testing so some form of automatic or remote pressure application would have to be used. Secondly, finding sensors and electronics which can survive the elevated temperatures could be challenging.

REFERENCES

American Society for Metals, ASM International. Handbook Committee. (1990). *Metals handbook: Volume 2*. Metals Park, Ohio: ASM International.

Baba, T., Ono, A. (2001). Improvement of the laser flash method to reduce uncertainty in thermal diffusivity measurements. Measurement Science and Technology, v 12, 2046–2057.

Bosch, E. G. T., Lasance, C. J. M. (2000). Accurate measurement of interface thermal resistance by means of a transient method. *16th IEEE Semiconductor Thermal Measurement and Management Symposium*, 167-173.

Carlberg, B., Wang, T., Liu, J., Shangguan, D. (2009). Polymer-metal nano-composite films for thermal management. *Microelectronics International*, v26, 28–36.

Chomerics (2001), *CHO-THERM® 1671 insulators data sheet*. Retrieved from: http://www.chomerics.com/products/therm_chotherm.htm.

Chomerics (1999), *CHO-THERM® T500 insulators data sheet*. Retrieved from: http://www.chomerics.com/products/therm_chotherm.htm.

Clark III, L. M., Taylor, R. E. (1975). Radiation loss in the flash method for thermal diffusivity. *Journal of Applied Physics*, v46, 714-719.

deSorgo, M.(1996). Thermal interface materials. *Electronics Cooling Magazine*, Sept. 1996.

Gwinn, J. P., Webb, R. L. (2003). Performance and testing of thermal interface materials. *Microelectronics Journal*, v34, 215-222.

Khuu, V., Osterman, M., Bar-Cohen, A., Pecht, M. (2009). Effects of temperature cycling and elevated temperature/humidity on the thermal performance of thermal interface materials. *IEEE Transactions on Device and Materials Reliability*, v9, 379-391.

Laird Technologies (2010a). *Tgrease^TM 880 series thermal grease data sheet*. Retrieved from: http://www.lairdtech.com/Products/Thermal-Management-Solutions/ Thermal-Interface-Materials/Thermally-Conductive-Grease.

Laird Technologies (2010b). Tpcm^TM *HP105 series phase change material data sheet*. Retrieved from: http://www.lairdtech.com/Products/Thermal-Management-Solutions/Thermal-Interface-Materials/Phase-Change-TIMs.

Laird Technologies (2009). *Tflex^{TM} 700 series thermal gap filler data sheet*. Retrieved from: http://www.lairdtech.com/Products/Thermal-Management-Solutions/ Thermal-Interface-Materials/Thermal-Gap-Filler.

Laird Technologies (2012 retrieved). *Tmate^{TM} 2900 series phase change tim data sheet*. Retrieved from: http://www.lairdtech.com/Products/Thermal-Management-Solutions/Thermal-Interface-Materials/Phase-Change-TIMs.

Lasance, C. J. M., Murray, C. T., Saums, D. L., Rencz, M. (2006). Challenges in thermal interface material testing. *22nd Semiconductor Thermal Measurement and Management Symposium*, 42-50.

Lee, S., Early, M., Pellilo, M. (1997). Thermal interface material performance in microelectronics packaging applications. *Microelectronics Journal*, v28, 13-20.

Liu, C. H., Huang, H., Wu, Y., Fan, S. S. (2004). Thermal conductivity improvement of silicone elastomer with carbon nanotube loading. *Applied Physics Letters*, v84, 4248-4250.

Liu, Z., Chung, D. D. L. (2006). Boron nitride particle filled paraffin wax as a phase-change thermal interface material. *Journal of Electronic Packaging*, v128, 319-323.

Luo, X., Xu , Y., Chung, D. D. L. (2001). Thermal stability of thermal interface pastes, evaluated by thermal contact conductance measurement. *Journal of Electronic Packaging*, v123, 309-311.

Park, J., Taya, M. (2006). Design of thermal interface material with high thermal conductivity and measurement apparatus. *Journal of Electronic Packaging*, v128, 46-52.

Parker, W .J., Jenkins, R. J., Butler, C. P., Abbott, G. L. (1961). Flash method of determining thermal diffusivity, heat capacity, and thermal conductivity. *Journal of Applied Physics*, v32, 1679-1684.

Sarvar, F., Whalley, D. C., Conway, P. P. (2006). Thermal interface materials: A review of the state of the art. *Electronics System Integration Technology Conference*, 1292-1302.

Smith, B., Brunschwiler, T., Michel, B. (2009). Comparison of transient and static test methods for chip-to-sink thermal interface characterization. *Microelectronics Journal*, v40, 1379–1386.

Szekel, V. (1998). Identification of RC Networks by deconvolution: Chances and limits. *IEEE Transactions on Circuits and Systems I: Fundamental Theory and Application*, V45, 244-258.

Xu, Y., Luo, X., Chung, D. D. L., (2000). Sodium silicate based thermal interface material for high thermal contact conductance. *Journal of Electronic Packaging*, v122, 128-131.

Xu , Y., Luo, X., Chung, D. D. L. (2002). Lithium doped polyethylene-glycol-based thermal interface pastes for high thermal contact conductance. *Journal of Electronic Packaging*, v124, 188-191.

Xu, J., Fisher, T. S. (2006). Enhancement of thermal interface materials with carbon nanotube arrays. *International Journal of Heat and Mass Transfer*, v49, 1658–1666.

Zhang, K., Chai, Y., Yuen, M. M. F., Xiao, D.G.W., Chan, P.C.H. (2008). Carbon nanotube thermal interface material for high-brightness light-emitting-diode cooling. *Nanotechnology*, v19, 1-8.

APPENDIX A: MATLAB PROGRAM CODE USED TO CALCULATE THE INTERFACE CONDUCTANCE

This section contains the MatLab script used to calculate the conductance values. It consists of two separate files. The main file from which it is run, Data_Processing_Program_reve.m , and a function DataPoint_Processor.m. The main program cycles through the different data points in a data set and compiles the conductance and pressure measurements into a text file for plotting. The function DataPoint_Processor.m deals with the calculation of the conductance from a single set of temperature readings like shown in chapter 3.

Data_Processing_Program_reve.m

```matlab
close all
clear
clc

Revision='E'
%CALCULATE THE CONDUCTANCE AT EACH DATA POINT IN THE SET

Dataset='Dataset24_26_06_12_NoTIM_BlockB_t5';%This is name of dataset
being used
ndp=8; %# of data points in the set

%The function DataPoint_Processor is called to calculate the
conductance of
%each data point, the results are saved
for i=1:ndp
    output=DataPoint_Processor(Dataset, i);
    C(i)=output(1);%Conductance
    WC(i)=output(2);%Conductance uncertainty
    P(i)=output(3);%Pressure
    Q(i)=output(4);%Heat Transfer
end

%PLOT THE DATASET
scrsz = get(0,'ScreenSize');
plot1=figure('Position',[scrsz(3)/8 100 scrsz(3)*(3/4)
scrsz(4)*(3/4)]);
axes('FontSize', 12)
```

```matlab
plot(P, C,'sk','MarkerSize',6,'MarkerFaceColor','r')
hold all
hold all
errorbar(P, C, C.*WC)

xlabel('Pressure(psi)','FontSize', 12)
ylabel('Contact Conductance(W/cm^2K)','FontSize', 12)

%OUTPUT THE RESULTS TO A TEXT FILE FOR PLOTTING
fname='\Results_';
Address=[Dataset,fname,Dataset, '.txt'];
Output=fopen(Address,'wt');
for i=1:ndp
fprintf(Output,'%-10.3f     ', C(i));
fprintf(Output,'%-10.3f     ', WC(i));
fprintf(Output,'%-10.3f     ', P(i));
fprintf(Output,'%-10.3f\n', Q(i));
end
fprintf(Output,['\n\n',DATESTR(NOW),'\nRev ',Revision]);
fclose(Output);
```

DataPoint_Processor.m

_____

```matlab
function [output]=DataPoint_Processor(Dataset,dp)
%Revision E

%IMPORT DATA
Datapoint=['DataPoint',sprintf('%i',dp)];
Address=[Dataset,'\',Datapoint,'\inputdata.txt'];
Data=fopen(Address,'r');

i=1;
while feof(Data)==0
    date(i,:)=fscanf(Data, '%28c',1);
    data(i,:)=fscanf(Data, '%f ',8);
    i=i+1;
end
fclose(Data);
date
data
%IMPORT CALIBRATION CURVES
Address='Calibration.txt';
Cal=fopen(Address,'r');

prtd2=fgets(Cal);
prtd2=sscanf(prtd2,'%f');
prtd3=fgets(Cal);
prtd3=sscanf(prtd3,'%f');
prtd4=fgets(Cal);
prtd4=sscanf(prtd4,'%f');
prtd5=fgets(Cal);
```

87

```matlab
prtd5=sscanf(prtd5,'%f');
prtd6=fgets(Cal);
prtd6=sscanf(prtd6,'%f');

fclose(Cal);

%FIX DATA WITH CALIBRATION CURVES
datafix(:,1)=data(:,1);
datafix(:,2)=data(:,2);
datafix(:,3)=data(:,3)+polyval(prtd2,data(:,3));  %fixes the data file
according to the supplied calibration curves
datafix(:,4)=data(:,4)+polyval(prtd3,data(:,4));
datafix(:,5)=data(:,5)+polyval(prtd4,data(:,5));
datafix(:,6)=data(:,6)+polyval(prtd5,data(:,6));
datafix(:,7)=data(:,7)+polyval(prtd6,data(:,7));
datafix(:,8)=data(:,8);

datafix(:,1)=datafix(:,1)/60;  %%change to minutes

fontsize=12;
linewidth=2;

%PREVIEW PLOTS
scrsz = get(0,'ScreenSize');
plot1=figure('Position',[0 scrsz(4)/2 scrsz(3)/3 scrsz(4)/2.35]);
axes('FontSize', fontsize)
plot(datafix(:,1),datafix(:,2),datafix(:,1),datafix(:,3),datafix(:,1),d
atafix(:,4),datafix(:,1),datafix(:,5),datafix(:,1),datafix(:,6),datafix
(:,1),datafix(:,7), 'LineWidth', linewidth)
xlim([0 10]);
%title('Measured Temperatures vs Time')
xlabel('Time(min)','FontSize', fontsize)
ylabel('Temperature(C)','FontSize', fontsize)
legend('RTD1','RTD2','RTD3', 'RTD4', 'RTD5', 'RTD6', 'Location',
'East')

plot2=figure('Position',[scrsz(3)/3 scrsz(4)/2 scrsz(3)/3
scrsz(4)/2.35]);
axes('FontSize', fontsize)
plot(datafix(:,1),datafix(:,8), 'LineWidth', linewidth)
xlim([0 10]);
%title('Measured Pressure vs Time')
xlabel('Time(min)','FontSize', fontsize)
ylabel('Pressure(psi)','FontSize', fontsize)

%PREPROCESSING

l1=38.03;%CMD Measuresments
l2=25.35;
l3=12.62;
l4=12.58;
l5=25.29;
l6=38.00;
```

```matlab
a=0.000645; %m^2

k=167;%conductivity of the meterbars

sdata=size(datafix);

time=datafix(:,2);

Temp=datafix(:,2:7);

Pr=datafix(:,8);
SP=std(Pr);
P=mean(Pr);

%PLOT THE AVERAGE TEMPERATURE READINGS
Tavg(1)=mean(Temp(:,1));
Tavg(2)=mean(Temp(:,2));
Tavg(3)=mean(Temp(:,3));
Tavg(4)=mean(Temp(:,4));
Tavg(5)=mean(Temp(:,5));
Tavg(6)=mean(Temp(:,6));

d=[l1, l2, l3, l4, l5, l6];

[Tfithot,err] = polyfit(d(1:3),Tavg(1:3),1);
dfit=0:0.1:40;
Rcheck=polyval(Tfithot,[d(1:3)]);
RShot=corrcoef(Tavg(1:3),Rcheck);
Tfithotplot=polyval(Tfithot,dfit);

[Tfitcold,err] = polyfit(d(4:6),Tavg(4:6),1);
Rcheck=polyval(Tfitcold,[d(4:6)]);
RScold=corrcoef(Tavg(4:6),Rcheck);
Tfitcoldplot=polyval(Tfitcold,dfit);

plot3=figure('Position',[0 scrsz(4)/2 scrsz(3)/3 scrsz(4)/2.35]);
axes('FontSize', fontsize)
colour={'r' 'g' ' b' 'c' 'm' 'y'};
for i=1:6
    plot(d(i), Tavg(i),'sk','MarkerSize',6,'MarkerFaceColor',colour{i})
    hold all
end
plot(dfit,Tfithotplot,dfit,Tfitcoldplot,'--k')
hold all
xlim([0 40])
xlabel('Distance from Interface(mm)','FontSize', fontsize)
ylabel('Temperature(C)','FontSize', fontsize)
legend('RTD1','RTD2','RTD3', 'RTD4', 'RTD5', 'RTD6', 'Location',
'East')

%CALCULATE THE TEMPERATURE DROP ACROSS THE TIM
```

```
Ul=0.01;%mm
Udl=sqrt(Ul^2+Ul^2);%mm
Ua=0.1;%m^2
UdT=0.05;%K


[temp,nT]=size(Temp);


dT34=mean(Temp(:,3)-Temp(:,4));%K
SdT34=std(Temp(:,3)-Temp(:,4));%K
BdT34=UdT;
PdT34=1.96*SdT34/sqrt(nT);
WdT34=sqrt(BdT34^2+PdT34^2);%K


dT13=mean(Temp(:,1)-Temp(:,3));%K
SdT13=std(Temp(:,1)-Temp(:,3));%K
BdT13=UdT;
PdT13=1.96*SdT13/sqrt(nT);
WdT13=sqrt(BdT13^2+PdT13^2);%K


dT46=mean(Temp(:,4)-Temp(:,6));%K
SdT46=std(Temp(:,4)-Temp(:,6));%K
BdT46=UdT;
PdT46=1.96*SdT46/sqrt(nT);
WdT46=sqrt(BdT46^2+PdT46^2);%K


dTdxh=dT13/(l1-l3);%K/mm
WdTdxh=sqrt((WdT13/dT13)^2+(Udl/(l1-l3))^2);%relative


dTdxc=dT46/(l6-l4);%K/mm
WdTdxc=sqrt((WdT46/dT46)^2+(Udl/(l6-l4))^2);%relative


dT3h=dTdxh*l3;%K
WdT3h=sqrt((WdTdxh)^2+(Ul/l3)^2);%relative


dTc4=dTdxc*l4;%K
WdTc4=sqrt((WdTdxc)^2+(Ul/l4)^2);%relative


dThc=dT34-dT3h-dTc4;
WdThc=sqrt((WdT34)^2+(WdT3h*dT3h)^2+(WdTc4*dTc4)^2);%K



%CALCULATE THERMAL CONDUCTANCE
Q1=k.*a.*(dTdxh*1000);
Q2=k.*a.*(dTdxc*1000);
WQ=sqrt(WdTdxh^2);%relative
Q=(Q1+Q2)/2;
R=(a/Q)*(dThc);%m^2K/W
C=1/(R*10^4);  %W/cm^2K
WC=sqrt(WQ^2+(WdThc/dThc)^2);%relative

output=[C,WC,P,Q,dThc];
```

```
%Auto Save all Figures
saveas(plot1,[Dataset,'\',Datapoint,'\',Dataset,Datapoint,'_T_vs_time.t
iff'])
saveas(plot2,[Dataset,'\',Datapoint,'\',Dataset,Datapoint,'_P_vs_time.t
iff'])
saveas(plot3,[Dataset,'\',Datapoint,'\',Dataset,Datapoint,'_T_vs_locati
on.tiff'])


close all
```

APPENDIX B: COPYRIGHT PERMISSIONS

Included in this appendix are the copyright permissions held for figures used in Chapter 1 of this thesis: Fig. 1.1, 1.2, and 1.4.

Dear Mr. Sponagle,

It is our pleasure to grant you permission to publish the ASME **Figure 2** from "Design of thermal interface material with high thermal conductivity and measurement apparatus," by Park, J., Taya, M., Journal of Electronic Packaging, Volume 128, 2006, as cited in your letter for inclusion in a Masters Thesis entitled DETERMINATION OF THE THERMAL CONDUCTANCE OF THERMAL INTERFACE MATERIALS AS A FUNCTION OF PRESSURE LOADING to be published by Dalhousie University. As is customary, we request that you ensure full acknowledgment of this material, the author(s), source and ASME as original publisher. Acknowledgment must be retained on all pages printed and distributed.

Permission is granted for the specific use as stated herein and does not permit further use of the materials without proper authorization. Proper attribution must be made to the author(s) of the materials, and no alterations of the materials is permitted in any material manner. As is customary, we request that you ensure proper acknowledgment of the exact sources of this material, the authors, and ASME as original publisher. Acknowledgment must be retained on all pages printed and distributed.

In accordance with ASME policy, this permission is contingent upon payment of a royalty fee of **US$20 for 1 figure** (payment was made August 20, 2012). This is solely charged to non-authors of the requested ASME papers. We accept payments on all major credit cards such as: Visa, MasterCard, American Express, Discover, and Diners Club, or by check payable to ASME. Please send payment to the attention Michelle DeBlasi, ASME Accounting, 22 Law Drive, Fairfield, NJ 07007, and indicate that this is a permission payment. Should you have any questions regarding payment form or transfer, please contact Ms. DeBlasi; P: 973-244-2268, F: 973-882-4924; E:deblasim@asme.org.

Many thanks for your interest in ASME publications.

Sincerely,

Beth Darchi

Copyrights & Permissions

ASME International

Three Park Avenue

New York, NY 10016

P: 212-591-7700

F: 212-591-7292

E: darchib@asme.org

Supplier	Elsevier Limited The Boulevard,Langford Lane Kidlington,Oxford,OX5 1GB,UK
Registered Company Number	1982084
Customer name	Benjamin N Sponagle
Customer address	318-20 Charlotte Lane
	Halifax, NS b3m 4m1
License number	2963881306592
License date	Aug 07, 2012
Licensed content publisher	Elsevier
Licensed content publication	Microelectronics Journal
Licensed content title	Performance and testing of thermal interface materials
Licensed content author	J.P Gwinn,R.L Webb
Licensed content date	March 2003
Licensed content volume number	34
Licensed content issue number	3
Number of pages	8
Start Page	215
End Page	222
Type of Use	reuse in a thesis/dissertation
Portion	figures/tables/illustrations
Number of figures/tables/illustrations	2
Format	both print and electronic
Are you the author of this Elsevier article?	No
Will you be translating?	No
Order reference number	

94

Title of your thesis/dissertation	DETERMINATION OF THE THERMAL CONDUCTANCE OF THERMAL INTERFACE MATERIALS AS A FUNCTION OF PRESSURE LOADING
Expected completion date	Aug 2012
Estimated size (number of pages)	100
Elsevier VAT number	GB 494 6272 12
Permissions price	0.00 USD
VAT/Local Sales Tax	0.0 USD / 0.0 GBP
Total	0.00 USD
Terms and Conditions	

INTRODUCTION

1. The publisher for this copyrighted material is Elsevier. By clicking "accept" in connection with completing this licensing transaction, you agree that the following terms and conditions apply to this transaction (along with the Billing and Payment terms and conditions established by Copyright Clearance Center, Inc. ("CCC"), at the time that you opened your Rightslink account and that are available at any time at http://myaccount.copyright.com).

GENERAL TERMS

2. Elsevier hereby grants you permission to reproduce the aforementioned material subject to the terms and conditions indicated.

3. Acknowledgement: If any part of the material to be used (for example, figures) has appeared in our publication with credit or acknowledgement to another source, permission must also be sought from that source. If such permission is not obtained then that material may not be included in your publication/copies. Suitable acknowledgement to the source must be made, either as a footnote or in a reference list at the end of your publication, as follows:

"Reprinted from Publication title, Vol /edition number, Author(s), Title of article / title of chapter, Pages No., Copyright (Year), with permission from Elsevier [OR APPLICABLE SOCIETY COPYRIGHT OWNER]." Also Lancet special credit - "Reprinted from The Lancet, Vol. number, Author(s), Title of article, Pages No., Copyright (Year), with permission from Elsevier."

4. Reproduction of this material is confined to the purpose and/or media for which permission is hereby given.

5. Altering/Modifying Material: Not Permitted. However figures and illustrations may be altered/adapted minimally to serve your work. Any other abbreviations, additions, deletions and/or any other alterations shall be made only with prior written authorization of Elsevier Ltd. (Please contact Elsevier at permissions@elsevier.com)

6. If the permission fee for the requested use of our material is waived in this instance, please be advised that your future requests for Elsevier materials may attract a fee.

7. Reservation of Rights: Publisher reserves all rights not specifically granted in the combination of (i) the license details provided by you and accepted in the course of this licensing transaction, (ii)

these terms and conditions and (iii) CCC's Billing and Payment terms and conditions.

8. License Contingent Upon Payment: While you may exercise the rights licensed immediately upon issuance of the license at the end of the licensing process for the transaction, provided that you have disclosed complete and accurate details of your proposed use, no license is finally effective unless and until full payment is received from you (either by publisher or by CCC) as provided in CCC's Billing and Payment terms and conditions. If full payment is not received on a timely basis, then any license preliminarily granted shall be deemed automatically revoked and shall be void as if never granted. Further, in the event that you breach any of these terms and conditions or any of CCC's Billing and Payment terms and conditions, the license is automatically revoked and shall be void as if never granted. Use of materials as described in a revoked license, as well as any use of the materials beyond the scope of an unrevoked license, may constitute copyright infringement and publisher reserves the right to take any and all action to protect its copyright in the materials.

9. Warranties: Publisher makes no representations or warranties with respect to the licensed material.

10. Indemnity: You hereby indemnify and agree to hold harmless publisher and CCC, and their respective officers, directors, employees and agents, from and against any and all claims arising out of your use of the licensed material other than as specifically authorized pursuant to this license.

11. No Transfer of License: This license is personal to you and may not be sublicensed, assigned, or transferred by you to any other person without publisher's written permission.

12. No Amendment Except in Writing: This license may not be amended except in a writing signed by both parties (or, in the case of publisher, by CCC on publisher's behalf).

13. Objection to Contrary Terms: Publisher hereby objects to any terms contained in any purchase order, acknowledgment, check endorsement or other writing prepared by you, which terms are inconsistent with these terms and conditions or CCC's Billing and Payment terms and conditions. These terms and conditions, together with CCC's Billing and Payment terms and conditions (which are incorporated herein), comprise the entire agreement between you and publisher (and CCC) concerning this licensing transaction. In the event of any conflict between your obligations established by these terms and conditions and those established by CCC's Billing and Payment terms and conditions, these terms and conditions shall control.

14. Revocation: Elsevier or Copyright Clearance Center may deny the permissions described in this License at their sole discretion, for any reason or no reason, with a full refund payable to you. Notice of such denial will be made using the contact information provided by you. Failure to receive such notice will not alter or invalidate the denial. In no event will Elsevier or Copyright Clearance Center be responsible or liable for any costs, expenses or damage incurred by you as a result of a denial of your permission request, other than a refund of the amount(s) paid by you to Elsevier and/or Copyright Clearance Center for denied permissions.

LIMITED LICENSE

The following terms and conditions apply only to specific license types:

15. **Translation**: This permission is granted for non-exclusive world <u>**English**</u> rights only unless your license was granted for translation rights. If you licensed translation rights you may only translate this content into the languages you requested. A professional translator must perform all translations and reproduce the content word for word preserving the integrity of the article. If this license is to re-use 1 or 2 figures then permission is granted for non-exclusive world rights in all languages.

16. **Website**: The following terms and conditions apply to electronic reserve and author websites:
Electronic reserve: If licensed material is to be posted to website, the web site is to be password-protected and made available only to bona fide students registered on a relevant course if:
This license was made in connection with a course,
This permission is granted for 1 year only. You may obtain a license for future website posting,
All content posted to the web site must maintain the copyright information line on the bottom of each image,
A hyper-text must be included to the Homepage of the journal from which you are licensing at http://www.sciencedirect.com/science/journal/xxxxx or the Elsevier homepage for books at http://www.elsevier.com , and
Central Storage: This license does not include permission for a scanned version of the material to be stored in a central repository such as that provided by Heron/XanEdu.

17. **Author website** for journals with the following additional clauses:

All content posted to the web site must maintain the copyright information line on the bottom of each image, and the permission granted is limited to the personal version of your paper. You are not allowed to download and post the published electronic version of your article (whether PDF or HTML, proof or final version), nor may you scan the printed edition to create an electronic version. A hyper-text must be included to the Homepage of the journal from which you are licensing at http://www.sciencedirect.com/science/journal/xxxxx . As part of our normal production process, you will receive an e-mail notice when your article appears on Elsevier's online service ScienceDirect (www.sciencedirect.com). That e-mail will include the article's Digital Object Identifier (DOI). This number provides the electronic link to the published article and should be included in the posting of your personal version. We ask that you wait until you receive this e-mail and have the DOI to do any posting.

Central Storage: This license does not include permission for a scanned version of the material to be stored in a central repository such as that provided by Heron/XanEdu.

18. **Author website** for books with the following additional clauses:
Authors are permitted to place a brief summary of their work online only.
A hyper-text must be included to the Elsevier homepage at http://www.elsevier.com . All content posted to the web site must maintain the copyright information line on the bottom of each image. You are not allowed to download and post the published electronic version of your chapter, nor may you scan the printed edition to create an electronic version.

Central Storage: This license does not include permission for a scanned version of the material to be stored in a central repository such as that provided by Heron/XanEdu.

19. **Website** (regular and for author): A hyper-text must be included to the Homepage of the journal from which you are licensing at http://www.sciencedirect.com/science/journal/xxxxx or for books to the Elsevier homepage at http://www.elsevier.com

20. **Thesis/Dissertation**: If your license is for use in a thesis/dissertation your thesis may be submitted to your institution in either print or electronic form. Should your thesis be published commercially, please reapply for permission. These requirements include permission for the Library and Archives of Canada to supply single copies, on demand, of the complete thesis and include permission for UMI to supply single copies, on demand, of the complete thesis. Should your thesis be published commercially, please reapply for permission.

21. **Other Conditions**:

v1.6